IEEE Access
Multidisciplinary | Rapid Review | Open Access Journal

Received December 16, 2020, accepted January 15, 2021, date of publication February 2, 2021, date of current version March 3, 2021.

Digital Object Identifier 10.1109/ACCESS.2021.3056440

Optimal Geometry Analysis for Target Localization With Bayesian Priors

NGOC HUNG NGUYEN, (Member, IEEE)
Defence Science and Technology (DST) Group, Edinburgh, SA 5111, Australia
e-mail: ngoc.nguyen@dst.defence.gov.au

ABSTRACT Relative sensor-target geometry is well known to significantly affect the performance of target localization using a sensor network. This article analyzes the optimal sensor-target geometries for the problem of target localization with Bayesian priors. We present a unified geometry optimization framework for different types of sensor networks including bearing-only sensor network, range-only sensor network, received signal strength-only sensor network and mixed network of these sensor types. For geometry optimization of Bayesian target localization with these sensor networks, we establish the equivalence between the A-optimality criterion (i.e., minimizing the estimation mean squared error) and the D-optimality criterion (i.e., minimizing the area of the estimation uncertainty ellipse). Under these optimality criteria, the geometry optimization problem is shown to be mathematically equivalent to the problem of minimizing the modulus of a vector sum. This thus makes the optimal geometry conditions algebraically simple and easy to be computed. We conclude the article with extensive simulation studies to verify the accuracy of the analytical findings.

INDEX TERMS Optimal sensor placement, optimal geometry analysis, target localization, Bayesian estimation, information matrix.

I. INTRODUCTION

Target localization has been an area of significant interest for several decades due to its applications in many diverse areas including wireless communication networks, radar systems, search and rescue, and satellite positioning and navigation, to name but a few. The objective of target localization is to estimate the unknown position of a target from noisy measurements collected from multiple sensors. The relative sensor-target geometry is known in the target localization literature as an important factor that can significantly impact the estimation accuracy [1]–[3]. Therefore, it is crucial to determine the locations of the sensors to minimize the target position estimation uncertainty. Such a problem is commonly referred to as *optimal sensor placement*.

The existing literature on optimal sensor placement can be broadly categorized into (i) optimal control formulation and (ii) parameter optimization formulation [2], [4]. The former formulation is usually adopted for the problem of trajectory optimization for moving sensor platforms (commonly known as *optimal path planning*), where the objective is to minimize the target state estimation error under the optimal control framework [5]–[7]. On the other hand, given an initial estimate of the target position, the latter formulation aims to determine the optimal locations of the sensors such that the uncertainty of the target position estimation error is minimized [1]–[3]. This formulation is commonly known as *optimal geometry analysis*. Both formulations have pros and cons. Although the optimal control formulation can take into account various nonlinear physical and geometric constraints (e.g., minimum sensor-to-target clearance, obstacle and threat avoidance, and maximum communication sensor-to-sensor distance), this approach generally can only be solved via numerical methods. In contrast, the parameter optimization formulation can be analytically solved in most cases. Such closed-form analytical solutions reveal important insights into how the target estimation performance is affected by the relative sensor-target geometry and this knowledge is also helpful in developing tactical strategies for optimizing the sensor trajectory, such as to maximize fuel efficiency and maintain other physical and geometric constraints. Detailed discussions on the applications of the parameter optimization formulation (i.e., optimal geometry analysis) to cooperative target tracking can be found in [8].

The associate editor coordinating the review of this manuscript and approving it for publication was Gongbo Zhou.

Focusing on the parameter optimization formulation, optimal sensor-target geometries have been derived for various target localization problems including angle-of-arrival (i.e., bearing) based localization in [1], [2], [9]–[12], time-of-arrival (i.e., range) based localization in [1], [2], [12]–[18], time-difference-of-arrival based localization in [19], [20], received signal strength (RSS) based localization in [2], [12], [21], Doppler based localization in [22], [23], and hybrid-sensor based localization in [24]. In these works, the Cramér-Rao lower bound (CRLB) are used to characterize the target position estimation performance. Specifically, the D-optimality criterion (i.e., maximizing the determinant of the Fisher information matrix which is the inversion of the CRLB matrix) and the A-optimality criterion (i.e., minimizing the trace of the CRLB matrix) are the most commonly used criteria for geometry optimization. The D-optimality criterion effectively minimizes the area of the estimation uncertainty ellipse while the A-optimality criterion minimizes the estimation mean squared error (MSE).

An important underlying assumption of optimal geometry analysis is that an initial estimate of the target position has already been obtained and given from other means so that the optimal placement of the sensors can be determined based on this initial estimate [2]. However, in order to allow target localization to be formulated as a classical estimation problem (as if there is no prior information about the target position), the aforementioned works [1], [2], [9]–[24] ignored the uncertainty of the initial target position estimate; therefore, limiting the applicability of their analytical geometry results to practical tracking and localization systems.

To overcome the shortcoming of the existing works, in this article we consider the sensor-target geometry optimization problem under the Bayesian estimation framework to take into account the uncertainty in the prior knowledge of the target position. Specifically, the target position is modeled as a random variable following a given prior probability density function, and thus the target localization problem under consideration essentially becomes a Bayesian estimation problem. A work on geometry analysis under a similar setting was presented in [25] building upon the authors' previous works in [26], [27]. However, the solutions presented in [25] are somewhat ad hoc, particularly for the case of more than two sensors. The advantage of the current work is that we establish the equivalence between the A- and D-optimality criteria for geometry optimization of Bayesian localization and show that solving these optimality criteria are mathematically equivalent to minimizing the modulus of a vector sum. Intuitively, in the context of geometry optimization, the Bayesian priors can be viewed as an additional virtual sensor.

Given that the vector sum modulus minimization problem can be readily solved, our optimal geometry solutions are algebraically simpler than those presented in [25]. In addition, the optimality condition (12) in [25] is more restrictive than our proposed optimality condition. In particular, the optimality condition (12) in [25] is only a special case of our optimality condition when the modulus of the vector sum can be made zero. Using [9] as a reference, the optimality condition (12) in [25] is analogous to the *maximally optimal condition* in [9] while our proposed optimality condition is analogous to the more general *optimal condition* in [9] . The key contributions of this article are summarized as follows.

- A unified framework for optimal geometry analysis is presented for Bayesian target localization with different types of sensor networks: bearing-only sensor network, range-only sensor network, RSS-only sensor network, or mixed network of these sensor types.
- We establish an equivalence between the A-optimality criterion (i.e., minimizing the estimation MSE) and the D-optimality criterion (i.e., minimizing the area of the estimation uncertainty ellipse) for geometry optimization for Bayesian target localization using the above sensor networks.
- We show analytically that under the D-optimality (or equivalently A-optimality) criterion, the geometry optimization under consideration mathematically becomes the problem of minimizing the modulus of the sum of vectors, where one vector corresponds to a virtual sensor representing the Bayesian priors while the remaining vectors correspond to the sensors in the network. Once the solutions of the vector sum modulus minimization problem are found, the optimal placement of a sensor will be specified based on the orientation of the corresponding vector within the vector sum according to a certain rule depending on the sensor type. The vector sum modulus minimization can be readily solved and its solutions are also summarized in this article for the sake of completeness.
- Extensive simulation studies are presented to verify the accuracy of the analytical findings.

This article is organized as follows. Section II formulates and presents a unified framework for the problem of sensor-target geometry optimization for Bayesian target localization. The main analytical results of the article are provided in Section III. Comprehensive simulation studies are presented in Section IV. The article ends in Section V with concluding remarks.

Notations: Bold lower case letters/symbols represent vectors, while bold upper case letters/symbols denote matrices. Notations $(\cdot)^T$, $|\cdot|$ and trace$\{\cdot\}$ stand for matrix transpose, determinant and trace, respectively. The 4-quadrant arctangent is denoted by $\tan^{-1}(\cdot)$, and the Euclidean norm by $\|\cdot\|$. $\mathbf{A}(i,j)$ is the entry of matrix $\mathbf{A}$ at row i and column j, and diag$\{a_1,\ldots,a_N\}$ is a diagonal matrix with diagonal entries $a_1,\ldots,a_N$.

II. PROBLEM FORMULATION

A. TARGET LOCALIZATION WITH BAYESIAN PRIORS

Fig. 1 depicts the problem of localizing a stationary target using N spatially distributed sensors in $\mathbb{R}^2$ with Bayesian priors. We consider a general target localization problem, where each sensor collects one measurement that can be either

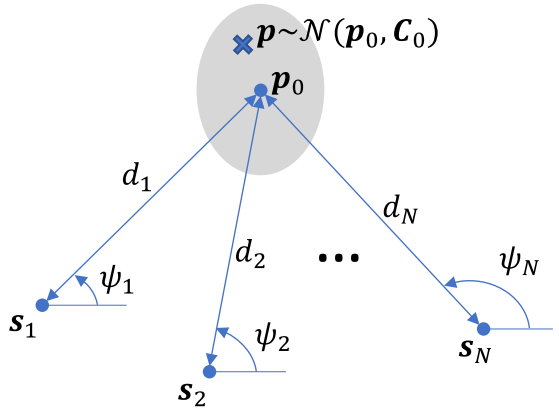

FIGURE 1. Localization geometry with Bayesian priors.

bearing (i.e., angle-of-arrival), range (i.e., time-of-arrival), or RSS. In other words, the sensor network can be a bearing-only network, a range-only network, a RSS-only network, or a mixed network of these sensor types. In Fig. 1, $\mathbf{p} = [p_x, p_y]^T$ is the unknown target position, and $\mathbf{s}_k = [s_{x,k}, s_{y,k}]^T$, $k = 1, \ldots, N$, is the position of sensor k. The target position $\mathbf{p}$ is modeled as a random variable following a given prior probability density function (PDF). The objective of Bayesian target localization is to estimate a particular realization of $\mathbf{p}$ from the available sensor measurements and the prior knowledge about the PDF of $\mathbf{p}$. In this article, $\mathbf{p}$ is assumed to be a Gaussian random variable. We denote $\mathbf{p} \sim \mathcal{N}(\mathbf{p}_0, \mathbf{C}_0)$, where $\mathbf{p}_0$ and $\mathbf{C}_0$ are the mean and covariance matrix of $\mathbf{p}$, respectively. Note that the grey ellipse in Fig. 1 illustrates the confidence region corresponding to the Bayesian priors. Using $\mathbf{p}_0 = [p_{x,0}, p_{y,0}]^T$ as a reference, the sensor position $\mathbf{s}_k$ can be specified using the distance $d_k = \|\mathbf{p}_0 - \mathbf{s}_k\|$ and the angle $\psi_k = \tan^{-1}\left(\frac{p_{y,0}-s_{y,k}}{p_{x,0}-s_{x,k}}\right)$.

The measurement model at sensor k can be expressed as

$$\tilde{z}_k = z_k + n_k = f_k(\mathbf{p}, \mathbf{s}_k) + n_k \tag{1}$$

where $z_k = f_k(\mathbf{p}, \mathbf{s}_k)$ is the noise-free measurement which is a nonlinear function of $\mathbf{p}$ and $\mathbf{s}_k$, and n_k is an independent zero-mean Gaussian noise, i.e., $n_k \sim \mathcal{N}(0, \sigma_k^2)$, accounting for the measurement noise at sensor k. Depending on the sensor types, the explicit expressions for measurement function f_k are given in Table 1. Note that we consider a general case where the measurement error variance σ_k^2 is completely arbitrary and can be different across the sensors.

Stacking $\tilde{z}_k$ for $k = 1, \ldots, N$ gives a vector form of the measurement model as

$$\tilde{\mathbf{z}} = \mathbf{z} + \mathbf{n} \tag{2}$$

where

$$\tilde{\mathbf{z}} = [\tilde{z}_1, \ldots, \tilde{z}_N]^T \tag{3a}$$
$$\mathbf{z} = [z_1, \ldots, z_N]^T = [f_1(\mathbf{p}, \mathbf{s}_1), \ldots, f_N(\mathbf{p}, \mathbf{s}_N)]^T \tag{3b}$$
$$\mathbf{n} = [n_1, \ldots, n_N]^T, \tag{3c}$$

and the covariance matrix of $\mathbf{n}$ is given by

$$\mathbf{R} = \mathbb{E}\{\mathbf{n}\mathbf{n}^T\} = \text{diag}\{\sigma_1^2, \ldots, \sigma_N^2\}. \tag{4}$$

The likelihood function of sensor measurements is a multivariate Gaussian probability density function, expressed by

$$\mathcal{L}(\tilde{\mathbf{z}}|\mathbf{p}) = \frac{1}{|2\pi\mathbf{R}|^{1/2}} \exp\left\{-\frac{1}{2}(\tilde{\mathbf{z}} - \mathbf{z})^T \mathbf{R}^{-1}(\tilde{\mathbf{z}} - \mathbf{z})\right\}. \tag{5}$$

The target localization problem under consideration can be solved by using the maximum a posteriori (MAP) estimator [28], [29]. The MAP estimator maximizes the posterior PDF $\mathcal{L}(\mathbf{p}|\tilde{\mathbf{z}})$, equivalently to

$$\begin{aligned}\hat{\mathbf{p}} &= \arg\max_{\mathbf{p}}\{\ln \mathcal{L}(\mathbf{p}|\tilde{\mathbf{z}})\} \\ &= \arg\max_{\mathbf{p}}\{\ln \mathcal{L}(\tilde{\mathbf{z}}|\mathbf{p}) + \ln \mathcal{L}(\mathbf{p})\}\end{aligned} \tag{6}$$

where $\ln \mathcal{L}(\tilde{\mathbf{z}}|\mathbf{p}) + \ln \mathcal{L}(\mathbf{p})$ is the Bayesian log-likelihood function. Here, $\ln \mathcal{L}(\mathbf{p})$ is given by

$$\mathcal{L}(\mathbf{p}) = \frac{1}{|2\pi\mathbf{C}_0|^{1/2}} \exp\left\{-\frac{1}{2}(\mathbf{p} - \mathbf{p}_0)^T \mathbf{C}_0^{-1}(\mathbf{p} - \mathbf{p}_0)\right\}. \tag{7}$$

Substituting (5) and (7) into (6), the MAP estimator becomes

$$\begin{aligned}\hat{\mathbf{p}} = \arg\min_{\mathbf{p}} \Big\{&(\tilde{\mathbf{z}} - \mathbf{z}(\mathbf{p}))^T \mathbf{R}^{-1}(\tilde{\mathbf{z}} - \mathbf{z}(\mathbf{p})) \\ &+ (\mathbf{p} - \mathbf{p}_0)^T \mathbf{C}_0^{-1}(\mathbf{p} - \mathbf{p}_0)\Big\}\end{aligned} \tag{8}$$

which can be solved using iterative search algorithms such as the Gauss-Newton algorithm [30], the steepest descent algorithm [31] and the Nelder-Mead simplex algorithm [32].

By linearizing $\mathbf{z}$, which is a function of $\mathbf{p}$, about the mean $\mathbf{p}_0$, an approximation for the covariance matrix of the target estimate $\hat{\mathbf{p}}$ is given by [25]

$$\begin{aligned}\mathbf{C}_{\hat{\mathbf{p}}} &= \mathbb{E}\left\{(\hat{\mathbf{p}} - \mathbf{p})(\hat{\mathbf{p}} - \mathbf{p})^T\right\} \\ &= \left(\mathbf{C}_0^{-1} + \mathbf{J}^T\mathbf{R}^{-1}\mathbf{J}\right)^{-1}\end{aligned} \tag{9}$$

where $\mathbf{J}$ is the Jacobian matrix of $\mathbf{z}(\mathbf{p})$ in (3b) with respect to $\mathbf{p}$ evaluated at $\mathbf{p} = \mathbf{p}_0$:

$$\mathbf{J} = \left[\mathbf{J}_1^T, \ldots, \mathbf{J}_N^T\right]^T \tag{10}$$

where

$$\mathbf{J}_k = \left[\frac{\partial f_k(\mathbf{p}, \mathbf{s}_k)}{\partial p_x}, \frac{\partial f_k(\mathbf{p}, \mathbf{s}_k)}{\partial p_y}\right]\Bigg|_{\mathbf{p}=\mathbf{p}_0}. \tag{11}$$

Taking the inversion of the covariance matrix $\mathbf{C}_{\hat{\mathbf{p}}}$, we obtain the information matrix as

$$\mathbf{M}_{\hat{\mathbf{p}}} = \mathbf{C}_{\hat{\mathbf{p}}}^{-1} = \mathbf{M}_0 + \mathbf{J}^T\mathbf{R}^{-1}\mathbf{J} \tag{12}$$

where $\mathbf{M}_0 = \mathbf{C}_0^{-1}$.

After some algebraic manipulations, the information matrix can be rewritten (see Appendix A) as

$$\mathbf{M}_{\hat{\mathbf{p}}} = \mathbf{M}_0 + \sum_{k=1}^{N} c_k^2 \mathbf{u}_k \mathbf{u}_k^T \tag{13}$$

TABLE 1. Measurement Models

Sensor type	Measurement function	Information matrix parameters
Bearing*	$z_k = f_k(\mathbf{p}, \mathbf{s}_k) = \tan^{-1}\left(\frac{p_y - s_{y,k}}{p_x - s_{x,k}}\right)$	$c_k^2 = \frac{1}{\sigma_k^2 d_k^2},\ \theta_k = \psi_k + \frac{\pi}{2}$
Range	$z_k = f_k(\mathbf{p}, \mathbf{s}_k) = \|\mathbf{p} - \mathbf{s}_k\|$	$c_k^2 = \frac{1}{\sigma_k^2},\ \theta_k = \psi_k$
RSS†	$z_k = f_k(\mathbf{p}, \mathbf{s}_k) = \gamma_0 - 10\alpha_k \log_{10}(\|\mathbf{p} - \mathbf{s}_k\|)$	$c_k^2 = \frac{100\alpha_k^2}{\ln^2(10)\sigma_k^2 d_k^2},\ \theta_k = \psi_k$

* $\tan^{-1}$ is the 4-quadrant arctangent.

† γ_0 is the RSS at the unit reference distance based on the free-space Friis model, and α_k is the signal path loss exponent.

where $\mathbf{u}_k$ is a unit vector defined by

$$\mathbf{u}_k = [\cos\theta_k, \sin\theta_k]^T. \tag{14}$$

Note that, depending on the sensor types, the expressions for parameters c_k and θ_k are given in Table 1.

B. GEOMETRY OPTIMIZATION AND CRITERION

The objective of this article is to analytically characterize the optimal sensor placement for target localization with Bayesian priors based on the A-optimality criterion (i.e., minimizing the estimation MSE) and the D-optimality criterion (i.e., minimizing the area of the estimation uncertainty ellipse). We will prove later in this section that these two criteria are in fact equivalent for the geometry optimization under consideration. To start with, we first consider the D-optimality criterion which is achieved by minimizing the area of the estimation uncertainty ellipse, or equivalently maximizing the determinant of the information matrix $\mathbf{M}_{\hat{\mathbf{p}}}$ in (13):

$$\begin{aligned}\{\mathbf{s}_1^{\text{opt}}, \ldots, \mathbf{s}_N^{\text{opt}}\} &= \underset{\{\mathbf{s}_1,\ldots,\mathbf{s}_N\}}{\arg\max} \left\{\left|\mathbf{M}_{\hat{\mathbf{p}}}\right|\right\} \\ &= \underset{\{\mathbf{s}_1,\ldots,\mathbf{s}_N\}}{\arg\max} \left\{\left|\mathbf{M}_0 + \sum_{k=1}^{N} c_k^2 \mathbf{u}_k \mathbf{u}_k^T\right|\right\}. \end{aligned} \tag{15}$$

We observed from (14) and Table 1 that the unit vector $\mathbf{u}_k$ only depends on the *'angular'* placement of the sensors with respect to $\mathbf{p}_0$ (i.e., being a function of the angle ψ_k). On the other hand, the coefficient c_k^2 is dependent on the measurement noise variance σ_k^2 and the target-sensor distance d_k for the bearing and RRS sensors, while is only dependent on σ_k^2 for the case of the range sensor. As a result, to facilitate the derivation of optimal geometry, it is commonly assumed in the literature that the coefficient c_k^2 is *arbitrary but fixed* and the geometry optimization problem boils down to optimizing the angular placement of the sensors:

$$\{\psi_1^{\text{opt}}, \ldots, \psi_N^{\text{opt}}\} = \underset{\{\psi_1,\ldots,\psi_N\}}{\arg\max} \left\{\left|\mathbf{M}_{\hat{\mathbf{p}}}\right|\right\}. \tag{16}$$

It is important to note that the geometry optimization problem becomes unbounded if the coefficient c_k^2 is unconstrained. Specifically, for the cases of bearing-only sensors, RSS-only sensors, or a mixed combination of bearing, RSS and range sensors, the optimal placement is obtained when the target-sensor distance d_k approaches zero (i.e., when c_k^2 tends to infinity). For the case of range-only sensors, the target-sensor distance does not affect the information matrix and thus has no influence on the optimality of sensor placement if the measurement noise variance σ_k^2 is fixed.

In what follows, we establish the equivalence between the D-optimality criterion (minimizing the area of the uncertaintly ellipse, or equivalently maximizing the determinant of the information matrix) and the A-optimality criterion (minimizing the MSE, or equivalently minimizing the trace of the estimation error covariance matrix).

Theorem 1: For constant c_k^2, the maximization of the determinant of the information matrix (i.e., minimizing the area of the uncertainty ellipse) is equivalent to the minimization of the trace of the estimation error covariance matrix (i.e., minimizing the MSE).

Proof: The estimation error covariance matrix can be rewritten as

$$\mathbf{C}_{\hat{\mathbf{p}}} = \mathbf{M}_{\hat{\mathbf{p}}}^{-1} = \frac{1}{|\mathbf{M}_{\hat{\mathbf{p}}}|}\begin{bmatrix} \mathbf{M}_{\hat{\mathbf{p}}}(2,2) & -\mathbf{M}_{\hat{\mathbf{p}}}(1,2) \\ -\mathbf{M}_{\hat{\mathbf{p}}}(2,1) & \mathbf{M}_{\hat{\mathbf{p}}}(1,1) \end{bmatrix} \tag{17}$$

with $\mathbf{M}_{\hat{\mathbf{p}}}(i,j)$ denoting the ith-row jth-column entry of $\mathbf{M}_{\hat{\mathbf{p}}}$. Note that $\mathbf{M}_{\hat{\mathbf{p}}}(1,2) = \mathbf{M}_{\hat{\mathbf{p}}}(2,1)$. The MSE is given by the trace of $\mathbf{C}_{\hat{\mathbf{p}}}$ as

$$\text{MSE} = \text{trace}\{\mathbf{C}_{\hat{\mathbf{p}}}\} = \frac{\mathbf{M}_{\hat{\mathbf{p}}}(1,1) + \mathbf{M}_{\hat{\mathbf{p}}}(2,2)}{|\mathbf{M}_{\hat{\mathbf{p}}}|}. \tag{18}$$

Substituting (14) into (13) yields

$$\mathbf{M}_{\hat{\mathbf{p}}} = \mathbf{M}_0 + \sum_{k=1}^{N} c_k^2 \begin{bmatrix} \cos^2\theta_k & \sin\theta_k\cos\theta_k \\ \sin\theta_k\cos\theta_k & \sin^2\theta_k \end{bmatrix}. \tag{19}$$

From (18) and (19), we have

$$\text{MSE} = \text{trace}\{\mathbf{C}_{\hat{\mathbf{p}}}\} = \frac{\text{trace}\{\mathbf{M}_0\} + \sum_{k=1}^{N} c_k^2}{|\mathbf{M}_{\hat{\mathbf{p}}}|}. \tag{20}$$

Therefore, for fixed c_k^2, the trace of the error covariance matrix and thus the MSE are minimized if and only if the determinant of the information matrix is maximized. □

Observation 1: The information matrix remains unchanged by moving a sensor from $\mathbf{s}_k$ to $2\mathbf{p}_0 - \mathbf{s}_k$ (i.e., reflecting the sensor about the target position prior mean $\mathbf{p}_0$). This is a very handy property that allows new optimal geometries to be generated from a given optimal geometry by reflecting one or more sensors about the target position prior mean.

Proof: In (13), substituting $2\mathbf{p}_0 - \mathbf{s}_k$ for $\mathbf{s}_k$ makes $\mathbf{u}_k$ become $-\mathbf{u}_k$, which does not change the information matrix. □

III. OPTIMAL GEOMETRY ANALYSIS

The optimal angular sensor-target geometry for Bayesian target localization is governed by the following theorem.

Theorem 2: Suppose that the coordinate system is rotated without loss of generality such that the prior information matrix $\mathbf{M}_0$ *is diagonal*

$$\mathbf{M}_0 = \begin{bmatrix} A & 0 \\ 0 & B \end{bmatrix} \tag{21}$$

with $A > B$. *Then the maximization of the determinant of the information matrix is equivalent to*

$$\min_{\{\beta_1,\ldots,\beta_N\}} \left\{ \left\| \sum_{k=0}^{N} c_k^2 \mathbf{a}_k \right\|^2 \right\} \text{ with } \mathbf{a}_k = \begin{bmatrix} \cos\beta_k \\ \sin\beta_k \end{bmatrix} \tag{22}$$

where $c_0^2 = A - B$, $\beta_0 = 0$ *(i.e.,* $\mathbf{a}_0 = [1, 0]^T$*), and* $\beta_k = 2\theta_k$ *for* $k \in \{1, \ldots, N\}$.

Proof: By substituting (21) into (19) and calculating the determinant of $\mathbf{M}_{\hat{\mathbf{p}}}$, we obtain (see Appendix B for a detailed derivation)

$$\begin{aligned} |\mathbf{M}_{\hat{\mathbf{p}}}| = {} & AB + \frac{1}{2}(A+B)\sum_{k=1}^{N} c_k^2 \\ & + \frac{1}{4}\left(\sum_{k=1}^{N} c_k^2\right)^2 + \left(\frac{A-B}{2}\right)^2 \\ & - \frac{1}{4}\left((A-B) + \sum_{k=1}^{N} c_k^2 \cos 2\theta_k\right)^2 \\ & - \frac{1}{4}\left(\sum_{k=1}^{N} c_k^2 \sin 2\theta_k\right)^2. \end{aligned} \tag{23}$$

Using c_0^2, β_0 and $\beta_1, \ldots, \beta_N$ defined above, we can reexpress (23) as

$$\begin{aligned} |\mathbf{M}_{\hat{\mathbf{p}}}| = {} & AB + \frac{1}{2}(A+B)\sum_{k=1}^{N} c_k^2 \\ & + \frac{1}{4}\left(\sum_{k=1}^{N} c_k^2\right)^2 + \left(\frac{A-B}{2}\right)^2 \\ & - \frac{1}{4}\left(\sum_{k=0}^{N} c_k^2 \cos\beta_k\right)^2 - \frac{1}{4}\left(\sum_{k=0}^{N} c_k^2 \sin\beta_k\right)^2 \end{aligned} \tag{24}$$

Since $|\mathbf{M}_{\hat{\mathbf{p}}}| \geq 0$ while A, B and c_k^2 are fixed, maximizing $|\mathbf{M}_{\hat{\mathbf{p}}}|$ is equivalent to minimizing

$$\left(\sum_{k=0}^{N} c_k^2 \cos\beta_k\right)^2 + \left(\sum_{k=0}^{N} c_k^2 \sin\beta_k\right)^2 \tag{25}$$

over β_k, which is identical to (22). □

Remark 1: Once the minimization problem (22) is solved, the angular placement of each sensor is given by

$$\psi_k^{\text{opt}} = \begin{cases} \beta_k^{\text{opt}}/2 - \pi/2, & \text{for bearing sensor} \\ \beta_k^{\text{opt}}/2, & \text{for range or RSS sensor} \end{cases} \tag{26}$$

where β_k^{opt}, $k = 1, \ldots, N$, denotes the solution of (22).

Remark 2: The Bayesian priors influence the optimal geometry analysis via the additional term c_0^2 and $\mathbf{a}_0 = [1, 0]^T$ (i.e., $\beta_0 = 0$). In the context of geometry optimization, we can intuitively view the Bayesian priors as an additional virtual sensor which is characterized by c_0^2 and $\mathbf{a}_0$. It is important to note that this intuition only applies in the context of geometry optimization and is not valid in the general context of Bayesian target localization.

Remark 3: For the special case of $A = B$, we have $c_0^2 = 0$ and the minimization problem in (22) reduces to

$$\min_{\{\beta_1,\ldots,\beta_N\}} \left\{ \left\| \sum_{k=1}^{N} c_k^2 \mathbf{a}_k \right\| \right\}. \tag{27}$$

Note that, different to (22), the starting index of the summation within the minimization operation in (27) is 1 instead of 0. Therefore, the Bayesian priors have no influence on the optimal geometry analysis and the geometry optimization problem mathematically boils down to that of the classical non-Bayesian target localization in [1]. This is intuitively logical because the uncertainty ellipse of the priors becomes a circle when $A = B$ and thus gives no preference in terms of prior information toward any angular direction. As a result, the Bayesian priors play no role in the optimality of the angular sensor placement in this case.

Remark 4: The optimality condition stated in (22) of Theorem 2 is more general than the optimality condition (12) of [25]. Note that the optimal condition (22) in Theorem 2 reduces to the condition (12) of [25] only if

$$\min_{\{\beta_1,\ldots,\beta_N\}} \left\{ \left\| \sum_{k=0}^{N} c_k^2 \mathbf{a}_k \right\| \right\} = 0 \tag{28}$$

which is not always feasible. In general, the minimum value in (22) can be greater than zero.

Remark 5: The optimal geometry analysis presented in this article is also applicable to the problem of 2D Doppler-based localization where the position of a stationary target is estimated using Doppler-shift measurements collected from moving sensor platforms as considered in [22]. This is because the information matrix for such Doppler localization problem can be expressed in the form (13) by defining $c_k^2 = \omega_k^2/\sigma_k^2$ (ω_k is the angular velocity of sensor k with respect

to the target) and $\theta_k = \psi_k + \pi/2$. In contrast, it is not straightforward to extend the presented geometry analysis to the 2D Doppler-based localization problem of a moving target as considered in [23] (where the target position and velocity are estimated using Doppler-shift measurements collected from stationary sensors) since the information matrix in this case has a unique structure and cannot be re-expressed in the form (13).

A. SOLUTION OF OPTIMALITY CONDITIONS

The beauty of Theorem 2 is that it mathematically converts the Bayesian localization geometry optimization problem into the vector sum modulus minimization problem whose solutions can be readily obtained. In what follows, the solutions of vector sum modulus minimization will be summarized for the sake of completeness. Interested readers are referred to [1], [9] for detailed proofs and analyses of vector sum modulus minimization.

1) $N = 1$

The solution for (22) is given by

$$\beta_1^{\text{opt}} = \pm\pi. \tag{29}$$

Specifically, $\mathbf{a}_1$ is pointing in the opposite direction to $\mathbf{a}_0$, i.e.,

$$\mathbf{a}_1 = -\mathbf{a}_0. \tag{30}$$

2) $N \geq 2$

Theorem 3: If the condition of

$$c_j^2 \leq \sum_{i=0, i\neq j}^{N} c_i^2 \tag{31}$$

holds for all $j \in \{0, 1, \ldots, N \geq 2\}$, the minimization (22) for $N \geq 2$ is achieved if and only if the following condition is satisfied:

$$\sum_{k=0}^{N} c_k^2 \mathbf{a}_k = \mathbf{0}. \tag{32}$$

Otherwise, if there exists $j \in \{0, \ldots, N \geq 2\}$ such that

$$c_j^2 > \sum_{i=0, i\neq j}^{N} c_i^2, \tag{33}$$

the condition (32) is unsolvable and the minimization (22) for $N \geq 2$ is obtained by placing $\mathbf{a}_j$ in the opposite direction to the other vectors, i.e.,

$$\mathbf{a}_i = -\mathbf{a}_j \text{ for } i \in \{0, \ldots, N \geq 2\} \setminus j, \tag{34}$$

or

$$\beta_i^{\text{opt}} = \beta_j^{\text{opt}} \pm \pi \text{ for } i \in \{0, \ldots, N \geq 2\} \setminus j. \tag{35}$$

Proof: Please refer to the proofs of Theorems 8 and 9 in [1]. □

For $N = 2$, if the condition (31) holds, the solution of (32) is given by

$$\beta_1^{\text{opt}} = \pm\tan^{-1}(\sqrt{\zeta}, \kappa_2^2 - \kappa_1^2 - 1) \tag{36a}$$

$$\beta_2^{\text{opt}} = \mp\tan^{-1}(\sqrt{\zeta}, \kappa_1^2 - \kappa_2^2 - 1) \tag{36b}$$

$$\kappa_1 = (c_1/c_0)^2, \kappa_2 = (c_2/c_0)^2 \tag{36c}$$

$$\zeta = -\Big((\kappa_1+\kappa_2)^2 - 1\Big)\Big((\kappa_1-\kappa_2)^2 - 1\Big). \tag{36d}$$

For $N = 3$, if the condition (31) holds, the solution for (32) is governed by the following relationship between β_1^{opt}, β_2^{opt} and β_3^{opt}:

$$\beta_2^{\text{opt}} = \tan^{-1}\left(\frac{\varrho_1\vartheta_1 \pm \sqrt{\zeta}\varrho_2}{\kappa_1 \sin\beta_1^{\text{opt}}}, -\Big(\varrho_2\vartheta_1 \pm \sqrt{\zeta}\Big)\right) \tag{37a}$$

$$\beta_3^{\text{opt}} = \tan^{-1}\left(\frac{\varrho_1\vartheta_2 \mp \sqrt{\zeta}\varrho_2}{\kappa_1 \sin\beta_1^{\text{opt}}}, -\Big(\varrho_2\vartheta_2 \mp \sqrt{\zeta}\Big)\right) \tag{37b}$$

where

$$\zeta = \varrho_1(\vartheta_3^2 - 4\kappa_2^2\kappa_3^2), \tag{38a}$$

$$\varrho_1 = \kappa_1^2(\cos^2\beta_1^{\text{opt}} - 1), \varrho_2 = \kappa_1\cos\beta_1^{\text{opt}} + 1, \tag{38b}$$

$$\vartheta_1 = \kappa_1^2 + \kappa_2^2 - \kappa_3^2 + 2\kappa_1\cos\beta_1^{\text{opt}} + 1, \tag{38c}$$

$$\vartheta_2 = \kappa_1^2 - \kappa_2^2 + \kappa_3^2 + 2\kappa_1\cos\beta_1^{\text{opt}} + 1, \tag{38d}$$

$$\vartheta_3 = \kappa_1^2 - \kappa_2^2 - \kappa_3^2 + 2\kappa_1\cos\beta_1^{\text{opt}} + 1, \tag{38e}$$

$$\kappa_1 = c_1^2/c_0^2, \kappa_2 = c_2^2/c_0^2, \kappa_3 = c_3^2/c_0^2. \tag{38f}$$

Note that the value of β_1^{opt} can be chosen arbitrarily as long as ζ is positive, thus there exists infinitely many solutions for (32) when $N = 3$.

For $N \geq 3$, if the condition (31) is satisfied, the solution of (32) can be determined by splitting $\{\mathbf{a}_k\}_{k=0,\ldots,N}$ into smaller subset groups with two or three elements and then solving (32) for each subset group individually. Note that the splitting process must be carried out such that the condition (31) is also satisfied for all subset groups. The angular rotation between different optimally-configured subset groups will not affect the validity of the overall solution. Therefore, infinitely many solutions for (32) can be generated by rotating one or more optimally-configured subset groups.

IV. EXAMPLES AND NUMERICAL RESULTS

In this section, we present a range of examples and numerical results for various sensor network configurations to verify the analytical findings presented in Section III.

A. BEARING-ONLY SENSOR NETWORK

1) ONE BEARING SENSOR

Fig. 2(a) plots the determinant of the information matrix $|\mathbf{M}_{\hat{\mathbf{p}}}|$ with respect to the sensor angular placement ψ_1 for the case of one bearing sensor. The simulation parameters are $\mathbf{p}_0 = [0, 0]^T$ m, $\mathbf{C}_0 = \text{diag}\{12.1847, 24.3694\}$ m^2, $d_1 = 100$ m and $\sigma_1 = 2°$. We observe that $|\mathbf{M}_{\hat{\mathbf{p}}}|$ is maximized when $\psi_1^{\text{opt}} = 0$ and $\pm\pi$, corresponding to two optimal geometries shown in Figs. 2(b) and 2(c). Geometrically, an optimal geometry is formed when the line-of-sight (LOS) of the bearing sensor with respect to the target position prior mean is orthogonal to the major axis of the prior uncertainty

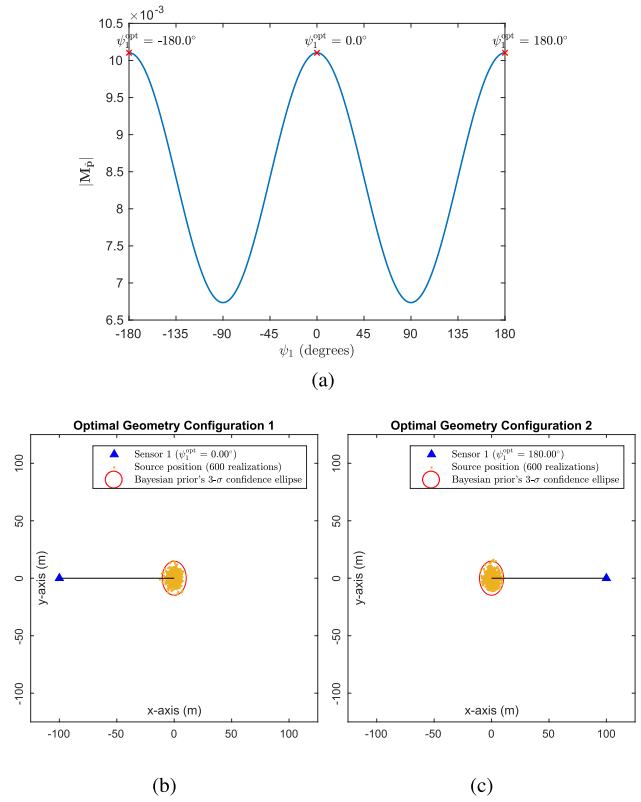

FIGURE 2. Optimal angular sensor placement for one bearing sensor: (a) The determinant of information matrix $|\mathbf{M}_{\hat{\mathbf{p}}}|$ as a function of ψ_1, and (b)–(c) Optimal geometry configurations. Parameter settings: $\mathbf{p}_0 = [0, 0]^T$ m, $\mathbf{C}_0 = \text{diag}\{12.1847, 24.3694\}$ m^2, $d_1 = 100$ m and $\sigma_1 = 2°$.

ellipse. This observation is consistent with the analytical findings in (26) and (29).

The maximum value of $|\mathbf{M}_{\hat{\mathbf{p}}}|$ is 10.103×10^{-3}, yielding a minimum root MSE (RMSE) of 4.506 m. Table 2 shows the bias and RMSE performance of the MAP estimator and the cubature transform (CT)-based bias-compensated Bayesian weighted instrumental variable estimator (BC-BWIVE-CT) [33] in the optimal geometry configurations shown in Fig. 2. In this simulation and throughout Section IV (unless otherwise stated), the bias and RMSE results are obtained from 100,000 Monte Carlo runs. The MAP estimator is implemented using the Gauss-Newton method [30] and is initialized to the target position prior mean $\mathbf{p}_0$. The Gauss-Newton algorithm halts after 30 iterations. We observe that the RMSEs of the BC-BWIVE-CT and MAP algorithms are approximately identical over the two optimal geometry configurations and closely match the optimal analytical RMSE value of 4.506 m.

2) TWO BEARING SENSORS

We now consider the case of two bearing sensors. The Bayesian priors are $\mathbf{p}_0 = [0, 0]^T$ m and $\mathbf{C}_0 = \text{diag}\{13.7266, 124.9122\}$ m^2. The target-sensor distances are $d_1 = 135$ m and $d_2 = 120$ m. The bearing noise standard deviations are set to $\sigma_1 = \sigma_2 = 1.5°$. In this scenario, the

TABLE 2. Bias and RMSE Performance for One Bearing Sensor Under the Optimal Geometries Shown in Fig. 2

	BC-BWIVE-CT		MAP	
Geometry	Bias norm	RMSE⋆	Bias norm	RMSE⋆
1	0.033 m	4.511 m	0.081 m	4.511 m
2	0.005 m	4.511 m	0.081 m	4.511 m

⋆Optimal RMSE = 4.506 m.

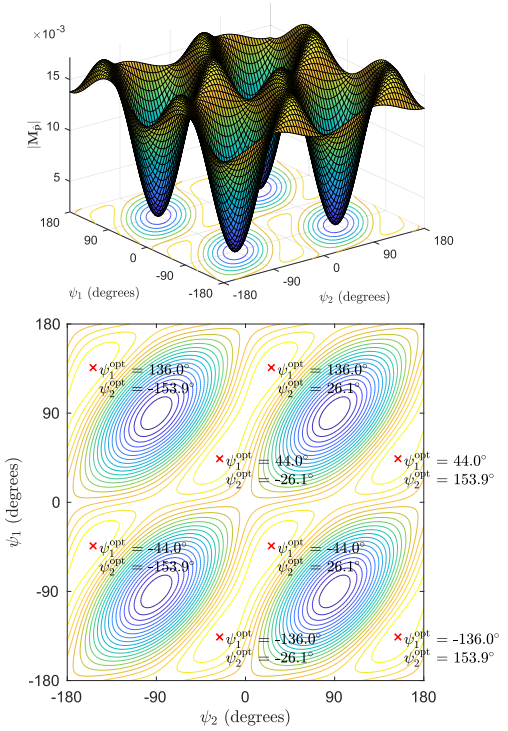

FIGURE 3. The determinant of information matrix $|\mathbf{M}_{\hat{\mathbf{p}}}|$ as a function of ψ_1 and ψ_2 for two bearing sensors (with maxima indicated by '×'). Parameter setting: $\mathbf{p}_0 = [0, 0]^T$ m, $\mathbf{C}_0 = \text{diag}\{13.7266, 124.9122\}$ m^2, $d_1 = 135$ m, $d_2 = 120$ m, and $\sigma_1 = \sigma_2 = 1.5°$.

condition (31) is satisfied. Thus, the solution for the optimal angular placement of the sensors can be obtained from (26) and (36), yielding $\{\psi_1^{\text{opt}}, \psi_2^{\text{opt}}\} = \{-44.04°, -153.92°\}$ and $\{-135.96°, -26.08°\}$. From these two solutions, Observation 1 can be used to generate 6 other optimal geometry configurations: $\{\psi_1^{\text{opt}}, \psi_2^{\text{opt}}\} = \{-44.04°, 26.08°\}$, $\{-135.96°, 153.92°\}$, $\{135.96°, 26.08°\}$, $\{44.04°, 153.92°\}$, $\{135.96°, -153.92°\}$, and $\{44.04°, -26.08°\}$. These 8 analytical geometry configurations match the maxima on the plot of the determinant of the information matrix $|\mathbf{M}_{\hat{\mathbf{p}}}|$ as shown in Fig. 3, thus confirming the accuracy of the analytical solution for $N = 2$ presented in Section III.

The optimal geometries are illustrated in Fig. 4. Note that there are only two distinct optimal geometry configurations in this case: configuration 1 and configuration 3. On the other hand, configurations 2 and 4 are just mirror images of configurations 1 and 3 over the y-axis, respectively; while configurations 1, 2, 3 and 4 will become configurations 5, 6, 7 and 8, respectively, if the coordinate system is rotated by 180°.

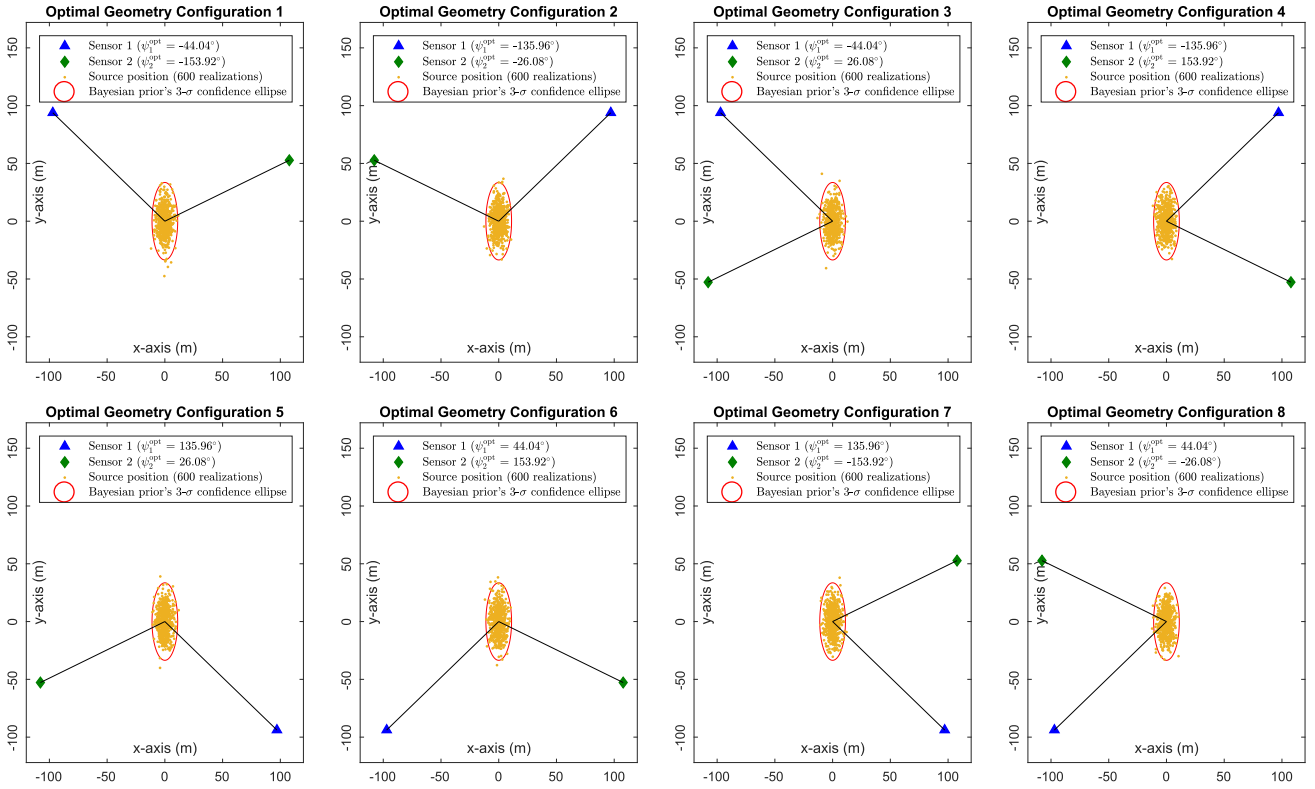

FIGURE 4. Optimal geometry configurations for two bearing sensors under the scenario and parameter settings given in Fig. 3.

TABLE 3. Bias and RMSE Performance for Two Bearing Sensors Under the Optimal Geometries Shown in Fig. 4

	BC-BWIVE-CT		MAP	
Geometry	Bias norm	RMSE*	Bias norm	RMSE*
1	0.007 m	3.936 m	0.052 m	3.933 m
2	0.006 m	3.940 m	0.051 m	3.937 m
3	0.009 m	3.920 m	0.070 m	3.916 m
4	0.009 m	3.914 m	0.070 m	3.910 m
5	0.007 m	3.936 m	0.052 m	3.932 m
6	0.007 m	3.938 m	0.052 m	3.934 m
7	0.009 m	3.912 m	0.070 m	3.907 m
8	0.009 m	3.901 m	0.070 m	3.897 m

*Optimal RMSE = 3.906 m.

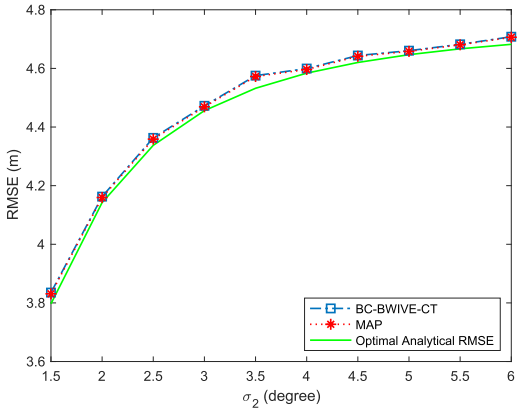

FIGURE 5. RMSE performance of the BC-BWIVE-CT and MAP estimators versus measurement noise for two bearing sensors.

The maximum value of $|\mathbf{M}_{\hat{\mathbf{p}}}|$ is 0.0172, yielding a minimum root MSE (RMSE) of 3.906 m. Table 3 reports the bias and RMSE performance of the BC-BWIVE-CT and MAP estimators under the optimal geometry configurations shown in Fig. 4. It is observed that the RMSEs of the BC-BWIVE-CT and MAP algorithms are approximately the same across different optimal geometry configurations and closely match the optimal analytical RMSE value of 3.906 m.

To further demonstrate the efficiency of the BC-BWIVE-CT and MAP estimators in the sense that they can attain the optimal analytical RMSE, Fig. 5 plots the empirical RMSE performance of these two estimators versus various values of $\sigma_2 \in \{1.5°, 2°, \ldots, 6°\}$ (i.e., the noise standard deviation of sensor 2). Other parameter settings remain unchanged as above. Note that, for each value of σ_2, an optimal geometry configuration is first determined according to (26) and (36), and the resulting geometry condition is then used to carry out Monte Carlo simulations with the BC-BWIVE-CT and MAP estimators. We observe in Fig. 5 that the RMSE curves of the BC-BWIVE-CT

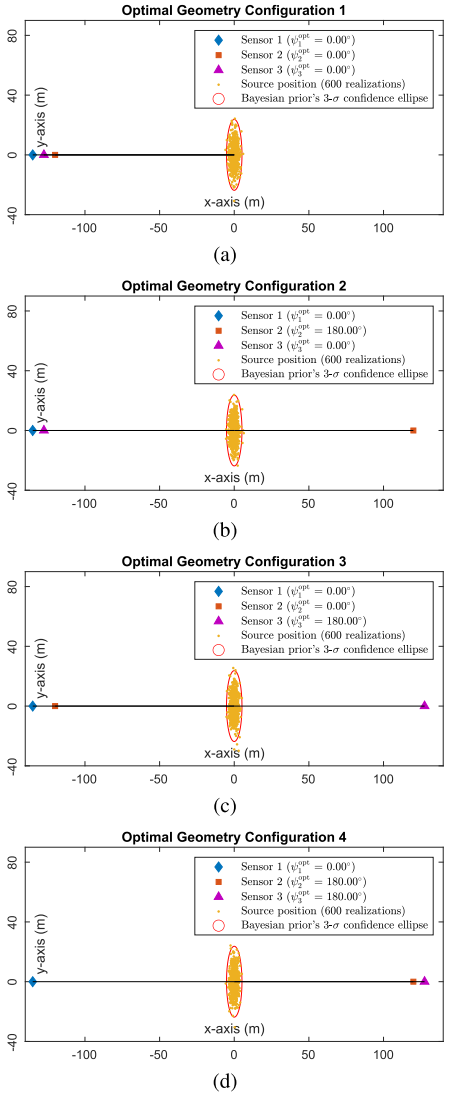

FIGURE 6. Optimal geometry configurations for three bearing sensors. Parameter setting: $\mathbf{p_0} = [0, 0]^T$ m, $\mathbf{C_0} = \text{diag}\{2.9741, 62.4561\}$ m^2, $d_1 = 135$ m, $d_2 = 120$ m, $d_3 = 127.5$ m, and $\sigma_1 = \sigma_2 = \sigma_3 = 1.5°$.

and MAP estimators both closely agree with the optimal analytical RMSE curve, thus confirming the efficiency of these algorithms.

3) THREE BEARING SENSORS

This example considers a sensor network with three bearing sensors for which the conditions (31) and (32) cannot be satisfied. The parameter settings are $\mathbf{p}_0 = [0, 0]^T$ m, $\mathbf{C}_0 = \text{diag}\{2.9741, 62.4561\}$ m^2, $d_1 = 135$ m, $d_2 = 120$ m, $d_3 = 127.5$ m, and $\sigma_1 = \sigma_2 = \sigma_3 = 1.5°$. Under this scenario, the condition (33) holds (i.e., $c_0^2 > c_1^2 + c_2^2 + c_3^2$). According to Theorem 3, the optimal geometry solutions are governed by $\mathbf{a}_1 = \mathbf{a_2} = \mathbf{a}_3 = -\mathbf{a}_0$. As a results, we obtain $\psi_1^{\text{opt}} \in \{0°, 180°\}$, $\psi_2^{\text{opt}} \in \{0°, 180°\}$, and $\psi_3^{\text{opt}} \in \{0°, 180°\}$, thus leading to 8 optimal configurations. Fig. 6 only shows 4 optimal configurations as the remaining configurations are simply mirror images of these configurations. Fig. 7 plots $|\mathbf{M}_{\hat{\mathbf{p}}}|$ as a function of ψ_2 and ψ_3 where ψ_1 is set to 0°. We observe that $|\mathbf{M}_{\hat{\mathbf{p}}}|$ attains it maximum values when $\psi_2^{\text{opt}} \in \{0°, 180°\}$ and $\psi_3^{\text{opt}} \in \{0°, 180°\}$, thus confirming the accuracy of the above analytical solutions. Table 4 reports the bias and RMSE performance of the BC-BWIVE-CT and MAP estimators under the geometries given in Fig. 6. The BC-BWIVE-CT and MAP estimators are observed to perform almost identically over these geometries and their RMSE performance closely agrees with the optimal value of 2.541 m.

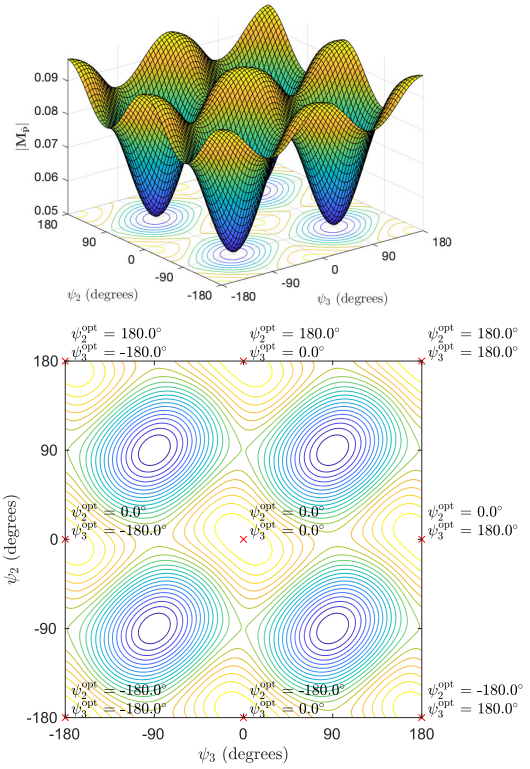

FIGURE 7. The determinant of information matrix $|\mathbf{M}_{\hat{\mathbf{p}}}|$ as a function of ψ_2 and ψ_3 for three bearing sensors with $\psi_1 = 0°$ under the scenario and parameter settings given in Fig. 6 (maxima indicated by '×').

TABLE 4. Bias and RMSE Performance for Three Bearing Sensors Under the Optimal Geometries Shown in Fig. 6

	BC-BWIVE-CT		MAP	
Geometry	Bias norm	RMSE⋆	Bias norm	RMSE⋆
1	0.028 m	2.548 m	0.022 m	2.547 m
2	0.005 m	2.546 m	0.005 m	2.546 m
3	0.006 m	2.544 m	0.008 m	2.543 m
4	0.016 m	2.541 m	0.009 m	2.541 m

⋆Optimal RMSE = 2.541 m.

B. RANGE-ONLY SENSOR NETWORK

1) ONE RANGE SENSOR

For the case of one range sensor, using (26) and (29), the optimal angular placement of the sensor is given by $\psi_1^{\text{opt}} = \pm\pi/2$. This analytical finding can be verified by observing in Fig. 8(a) that the determinant of the information

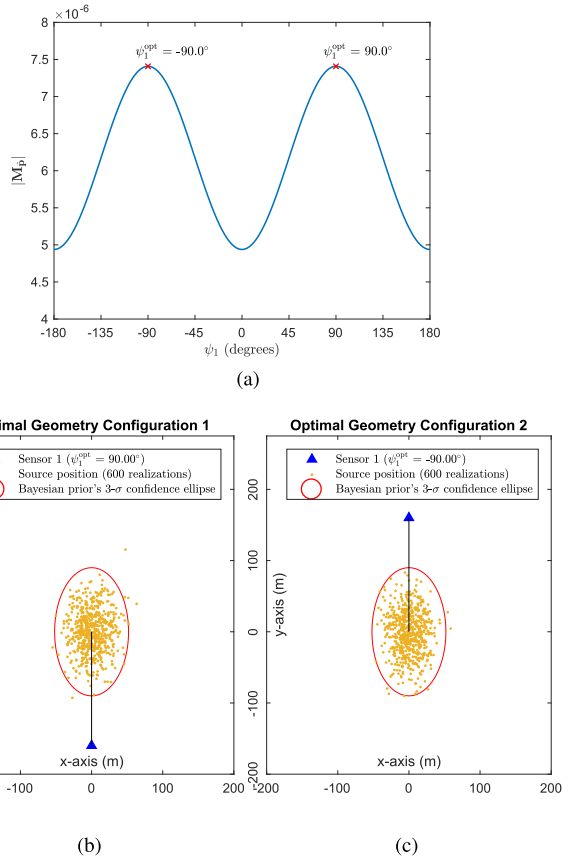

FIGURE 8. Optimal angular sensor placement for one range sensor: (a) The determinant of information matrix $|\mathbf{M}_{\hat{\mathbf{p}}}|$ as a function of ψ_1, and (b)–(c) Optimal geometry configurations. Parameter settings: $\mathbf{p}_0 = [0, 0]^T$ m, $\mathbf{C}_0 = \text{diag}\{300, 900\}$ m^2, $d_1 = 160$ m and $\sigma_1 = 30$ m.

TABLE 5. Bias and RMSE Performance of the MAP Estimator for One Range Sensor Under the Optimal Geometries Shown in Fig. 8

Geometry	Bias norm	RMSE*
1	0.480 m	27.455 m
2	0.483 m	27.468 m

*Optimal RMSE = 27.386 m.

matrix $|\mathbf{M}_{\hat{\mathbf{p}}}|$ attains its maximum values when $\psi_1^{\text{opt}} = \pm\pi/2$. The corresponding optimal geometries are shown in Figs. 8(b) and 8(c), in which the LOS of the range sensor with respect to the target position prior mean is orthogonal to the minor axis of the prior confidence ellipse. Table 5 reports the bias and RMSE performance of the MAP estimator under the optimal geometry configurations in Fig. 8. It is observed that the MAP estimator closely achieves the optimal analytical RMSE value under these two geometry conditions.

2) THREE RANGE SENSORS

We now consider a localization scenario with three range sensors and the following parameter settings: $\mathbf{p}_0 = [0, 0]^T$ m, $\mathbf{C}_0 = \text{diag}\{279.6961, 506.2500\}$ m^2, $d_1 = d_2 = d_3 = 160$ m, $\sigma_1 = 22.5$ m, $\sigma_2 = 17.5$ m and $\sigma_3 = 20$ m. Under this scenario, the condition (31) is met, thus the optimal angular placement of the sensor is governed by (26) and (37).

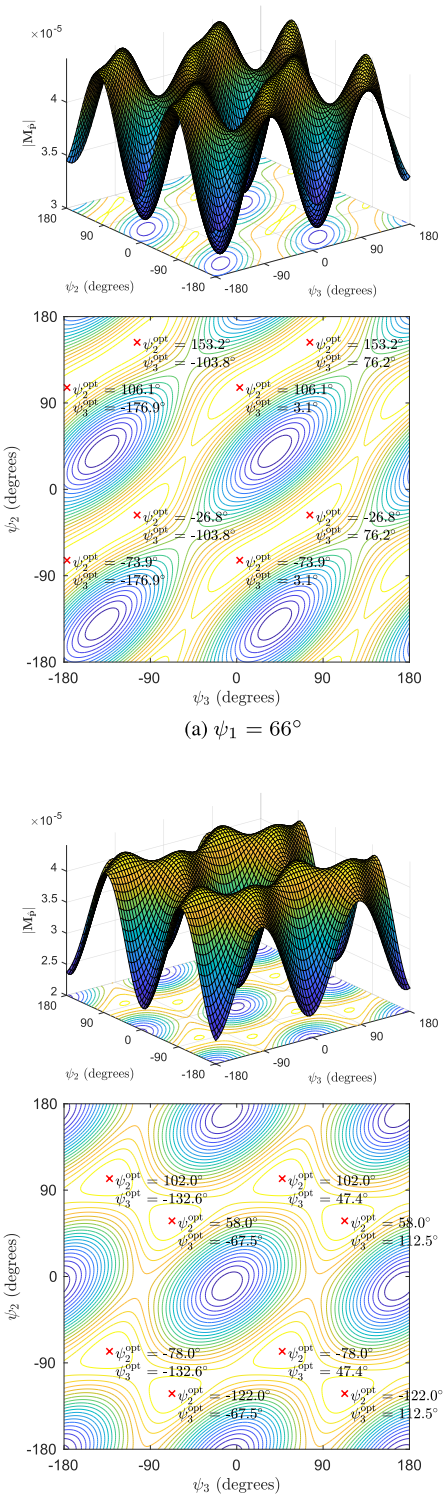

FIGURE 9. The determinant of information matrix $|\mathbf{M}_{\hat{\mathbf{p}}}|$ as a function of ψ_2 and ψ_3 for three range sensors (with maxima indicated by '×'). Parameter settings: $\mathbf{p}_0 = [0, 0]^T$ m, $\mathbf{C}_0 = \text{diag}\{279.6961, 506.2500\}$ m^2, $d_1 = d_2 = d_3 = 160$ m, $\sigma_1 = 22.5$ m, $\sigma_2 = 17.5$ m and $\sigma_3 = 20$ m.

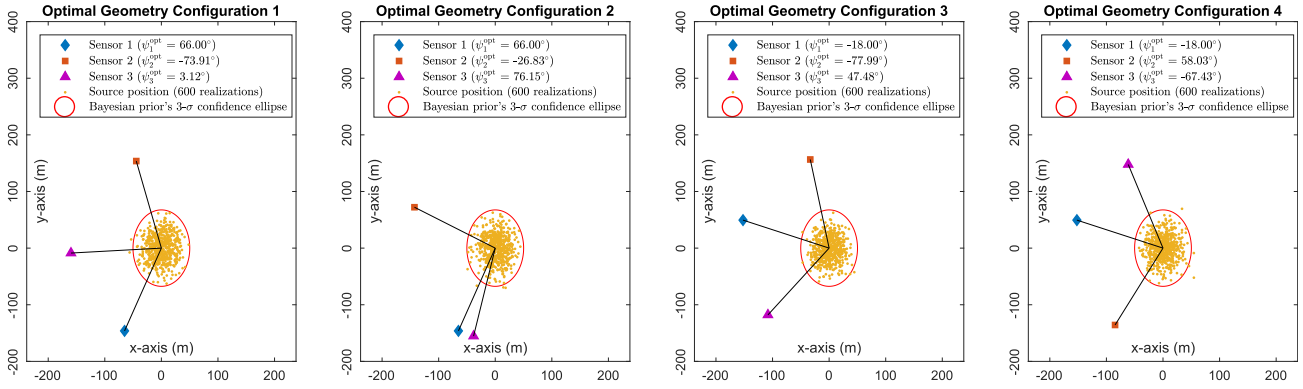

FIGURE 10. Examples of optimal geometry configurations for three range sensors under the scenario and parameter settings given in Fig. 9.

TABLE 6. Bias and RMSE Performance of the MAP Estimator for Three Range Sensors for the Optimal Geometries Shown in Fig. 10

Geometry	Bias norm	RMSE*
1	0.309 m	17.389 m
2	0.368 m	17.426 m
3	0.340 m	17.396 m
4	0.323 m	17.418 m

*Optimal RMSE = 17.348 m.

By arbitrarily setting $\psi_1 = 66°$, we obtain two solutions $\{\psi_2^{\text{opt}}, \psi_3^{\text{opt}}\} = \{-73.91°, 3.12°\}$ and $\{-26.83°, 76.15°\}$. These analytical solutions are consistent with two maxima of the determinant of the information matrix shown in Fig. 9(a). Note that, consistent with Observation 1, other maxima in Fig. 9(a) in fact can be generated from these two maxima by reflecting either sensor 2, sensor 3 or both of them about the target position prior mean. On the other hand, if $\psi_1 = -18°$, we obtain two solutions $\{\psi_2^{\text{opt}}, \psi_3^{\text{opt}}\} = \{58.03°, -67.43°\}$ and $\{-77.99°, 47.48°\}$. These analytical solutions agree with two maxima of the determinant of the information matrix shown in Fig. 9(b) while other maxima in Fig. 9(b) can be generated from these two maxima by reflecting either sensor 2, sensor 3 or both of them about the target position prior mean. These results verify the accuracy of the analytical solutions for $N = 3$ presented in Section III.

Fig. 10 plots four optimal geometry configurations corresponding to the above solutions, under which the determinant of the information matrix attains the maximum value of 4.4164×10^{-5} and the RMSE attains the minimum value of 17.348 m. Table 6 reports the bias and RMSE performance of the MAP estimator under the optimal geometry configurations shown in Fig. 10, where we observe that the MAP estimator performs almost identically over these geometries and its RMSE performance closely agrees with the optimal value of 17.348 m.

Fig. 11 plots the empirical RMSE performance of the MAP estimator against various values of $\sigma_3 \in \{15, 16, \ldots, 23\}$ m. Here, we set $\psi_1 = 66°$ while other parameter settings remain

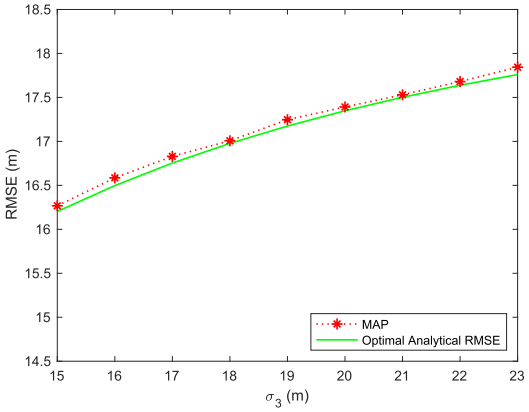

FIGURE 11. RMSE performance of the MAP estimator versus measurement noise for three range sensors.

TABLE 7. Bias and RMSE Performance of the MAP Estimator for One RSS Sensor Under the Optimal Geometries Shown in Fig. 12

Geometry	Bias norm	RMSE*
1	1.965 m	37.870 m
2	1.971 m	37.842 m

*Optimal RMSE = 37.938 m.

the same as above. For each value of σ_3, (26) and (37) are used to determine an optimal geometry configuration under which Monte Carlo simulations are then carried out to obtain the empirical RMSE performance of the MAP estimator. It is observed from Fig. 11 that the empirical RMSE curve of the MAP estimator closely agrees with the optimal analytical RMSE curve.

C. RSS-ONLY SENSOR NETWORK

1) ONE RSS SENSOR

Similar to the case of one range sensor, using (26) and (29), the optimal angular placement of one RSS sensor is $\psi_1^{\text{opt}} = \pm\pi/2$. Fig. 12 shows the determinant of the information matrix $|\mathbf{M}_{\hat{\mathbf{p}}}|$ as a function of ψ_1 and the geometry configurations for which $|\mathbf{M}_{\hat{\mathbf{p}}}|$ is maximized. The numerical results in Fig. 12 confirms the accuracy of the above analytical solution.

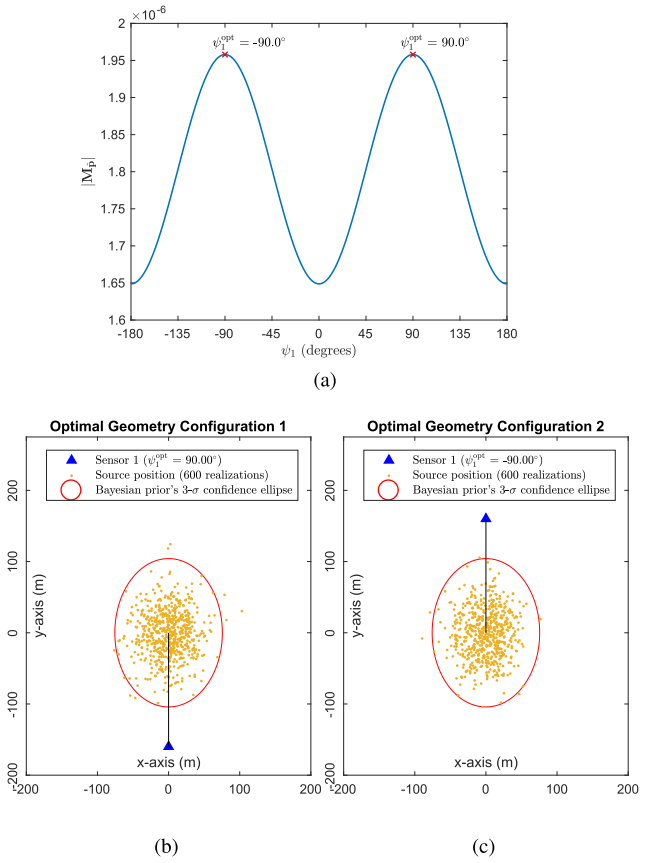

FIGURE 12. Optimal angular sensor placement for one RSS sensor: (a) The determinant of information matrix $|\mathbf{M}_{\hat{\mathbf{p}}}|$ as a function of ψ_1, and (b)–(c) Optimal geometry configurations. Parameter settings: $\mathbf{p}_0 = [0, 0]^T$ m, $\mathbf{C}_0 = \text{diag}\{634.9876, 1206.4764\}$ m^2, $\alpha_1 = 3$, $d_1 = 160$ m and $\sigma_1 = 4$ dBm.

Under the optimal sensor placement of $\psi_1^{\text{opt}} = \pm\pi/2$, the minimum RMSE is attained at the value of 37.938 m. It is observed in Table 7 that the MAP estimator yields RMSEs very close to this analytical RMSE value under the conditions of $\psi_1^{\text{opt}} = \pm\pi/2$.

2) TWO RSS SENSORS

Fig. 13 plots the determinant of the information matrix $|\mathbf{M}_{\hat{\mathbf{p}}}|$ as a function of ψ_1 and ψ_2 for the case of two RSS sensors with the parameter settings of $\mathbf{p}_0 = [0, 0]^T$ m, $\mathbf{C}_0 = \text{diag}\{610.7787, 1017.9644\}$ m^2, $\alpha_1 = \alpha_2 = 3$, $d_1 = 180$ m, $d_2 = 160$ m, $\sigma_1 = 4$ dBm and $\sigma_2 = 5$ dBm. We observe that $|\mathbf{M}_{\hat{\mathbf{p}}}|$ has four peaks located at $\{\psi_1^{\text{opt}}, \psi_2^{\text{opt}}\} = \{90°, 90°\}$, $\{90°, -90°\}$, $\{-90°, 90°\}$, $\{-90°, -90°\}$. This observation is consistent with the fact that the condition of $c_0^2 > c_1^2 + c_2^2$ holds in this scenario, and thus, according to Theorem 3 and Remark 1, an optimal geometry is obtained when both sensors are placed such that their LOSs are orthogonal to the minor axis of the prior confidence ellipse. These optimal geometry configurations are illustrated in Fig. 14. Under these geometries, $|\mathbf{M}_{\hat{\mathbf{p}}}|$ attains the maximum value of 2.579×10^{-6}, which leads to the minimum RMSE of 35.294 m. The bias and RMSE performance of the MAP estimator is reported in

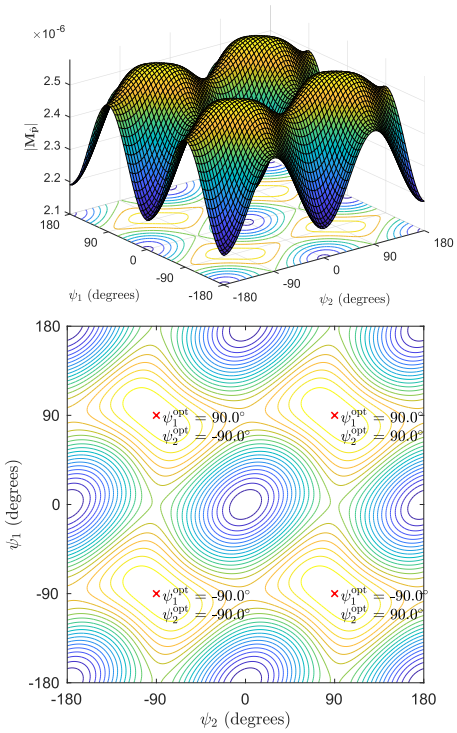

FIGURE 13. The determinant of information matrix $|\mathbf{M}_{\hat{\mathbf{p}}}|$ as a function of ψ_1 and ψ_2 for two RSS sensors (with maxima indicated by '×'). Parameter settings: $\mathbf{p}_0 = [0, 0]^T$ m, $\mathbf{C}_0 = \text{diag}\{610.7787, 1017.9644\}$ m^2, $\alpha_1 = \alpha_2 = 3$, $d_1 = 180$ m, $d_2 = 160$ m, $\sigma_1 = 4$ dBm, and $\sigma_2 = 5$ dBm.

TABLE 8. Bias and RMSE Performance of the MAP Estimator for Two RSS Sensors Under the Optimal Geometries Shown in Fig. 14

Geometry	Bias norm	RMSE*
1	1.469 m	35.224 m
2	0.044 m	35.195 m
3	0.052 m	35.180 m
4	1.472 m	35.251 m

*Optimal RMSE = 35.294 m.

Table 8, where we observe that the MAP estimator achieves a RMSE closely agreeing with the analytical RMSE in all the optimal geometry configurations.

Fig. 15 plots the empirical RMSE performance of the MAP estimator against various values of $\sigma_2 \in \{5, 5.5, \ldots, 10\}$ dBm (other parameter settings remain unchanged as above). Since the condition of $c_0^2 > c_1^2 + c_2^2$ holds for these values of σ_2, the optimal geometry solutions remain the same as those plotted in Fig. 14. Here, the empirical RMSE performance of the MAP estimator is obtained via 500,000 Monte Carlo runs under the geometry configuration shown in Fig. 14(a). The empirical RMSE curve of the MAP estimator is observed in Fig. 15 to closely match the optimal analytical RMSE curve.

3) FIVE RSS SENSORS

This example considers a sensor network with five RSS sensors. The parameter settings are $\mathbf{p}_0 = [0, 0]^T$ m,

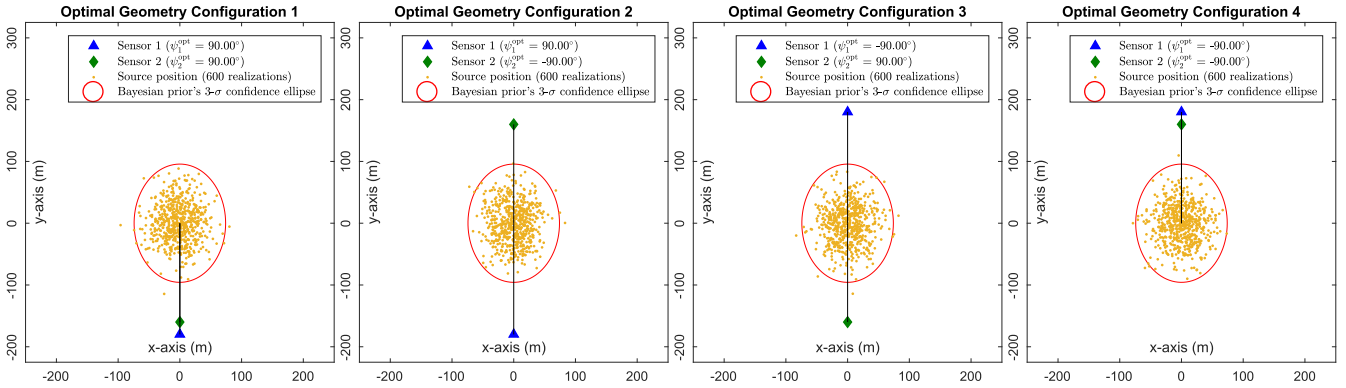

FIGURE 14. Optimal geometry configurations for two RSS sensors under the scenario and parameter settings given in Fig. 13.

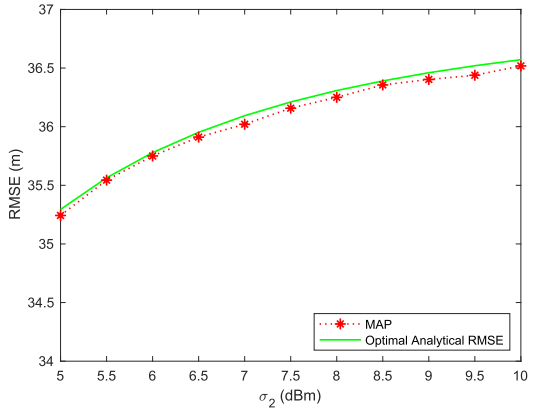

FIGURE 15. RMSE performance of the MAP estimator versus measurement noise for two RSS sensors.

$\mathbf{C}_0 = \text{diag}\{636.2278, 1017.9644\}$ m^2, $\alpha_1 = \cdots = \alpha_5 = 3$, $d_1 = 180$ m, $d_2 = 160$ m, $d_3 = 210$ m, $d_4 = 160$ m, $d_5 = 190$ m, $\sigma_1 = 4$ dBm, $\sigma_2 = 5$ dBm, $\sigma_3 = 3$ dBm, $\sigma_4 = 4.5$ dBm and $\sigma_5 = 5$ dBm. Since $N > 3$ and the condition (31) holds, the optimal sensor placement is governed by (32), whose solutions can be determined by splitting $\{\mathbf{a}_k\}_{k=0,\ldots,5}$ into smaller subset groups with two or three elements and then solving (32) for each subset group individually. In this example, we split $\{\mathbf{a}_k\}$ into two groups $\{\mathbf{a}_0, \mathbf{a}_1, \mathbf{a}_2\}$ and $\{\mathbf{a}_3, \mathbf{a}_4, \mathbf{a}_5\}$. The first group consists of the first two sensors and the virtual sensor corresponding to the Bayesian prior, while the second group include the three remaining sensors. The optimal arrangement between $\{\mathbf{a}_0, \mathbf{a}_1, \mathbf{a}_2\}$ can be determined using (36), where a particular solution is given by $\beta_1^{\text{opt}} = 174.58°$ and $\beta_2^{\text{opt}} = 186.70°$. Thus, we obtain $\psi_1^{\text{opt}} = 87.29°$ and $\psi_2^{\text{opt}} = 93.35°$. Similarly, using (36) results in an optimal arrangement between $\{\mathbf{a}_3, \mathbf{a}_4, \mathbf{a}_5\}$ governed by $\beta_4^{\text{opt}} - \beta_3^{\text{opt}} = 155.45°$ and $\beta_5^{\text{opt}} - \beta_3^{\text{opt}} = -133.66°$, thus leading to $\psi_4^{\text{opt}} - \psi_3^{\text{opt}} = 77.72°$ and $\psi_5^{\text{opt}} - \psi_3^{\text{opt}} = -66.83°$. Based on these results, an infinite number of optimal geometry configurations can be generated by rotating the second group (i.e., varying the value of ψ_3^{opt} from $-180°$ to $180°$).

TABLE 9. Bias and RMSE Performance of the MAP Estimator for Five RSS Sensors Under the Optimal Geometries Shown in Fig. 16

Geometry	Bias norm	RMSE⋆
1	1.511 m	31.204 m
2	0.170 m	31.159 m
3	1.122 m	31.128 m
4	1.391 m	31.270 m

⋆Optimal RMSE = 31.273 m.

Fig. 16 shows 4 optimal geometry examples for $\psi_3^{\text{opt}} = 36°$, $-100°$, $-21°$ and $131°$. Note that the reservation of the geometry optimality over the variation of ψ_3^{opt} is confirmed in Fig. 17, where we observe that the determinant of the information matrix remains constant regardless of ψ_3^{opt} given that $\psi_1^{\text{opt}} = 87.29°$, $\psi_2^{\text{opt}} = 93.35°$, $\psi_4^{\text{opt}} - \psi_3^{\text{opt}} = 77.72°$ and $\psi_5^{\text{opt}} - \psi_3^{\text{opt}} = -66.83°$. The maximum value of $|\mathbf{M}_{\hat{\mathbf{p}}}|$ is 4.1821×10^{-6}, and the corresponding minimum RMSE is 31.273 m. The RMSE performance of the MAP estimator under the optimal configurations in Fig. 16 is observed from Table 9 to closely match the optimal RMSE value.

Note that the splitting process can be carried out in different ways without affecting the optimality of the geometry solution. To demonstrate this, we now split $\{\mathbf{a}_k\}$ into two groups $\{\mathbf{a}_0, \mathbf{a}_1, \mathbf{a}_4\}$ and $\{\mathbf{a}_2, \mathbf{a}_3, \mathbf{a}_5\}$. By using (36), we obtain $\beta_1^{\text{opt}} = 154.16°$ and $\beta_4^{\text{opt}} = 205.84°$ (thus, $\psi_1^{\text{opt}} = 77.08°$ and $\psi_4^{\text{opt}} = 102.92°$) for the first group and $\beta_2^{\text{opt}} - \beta_3^{\text{opt}} = 163.82°$ and $\beta_5^{\text{opt}} - \beta_3^{\text{opt}} = -156.86°$ (thus, $\psi_2^{\text{opt}} - \psi_3^{\text{opt}} = 81.91°$ and $\psi_5^{\text{opt}} - \psi_3^{\text{opt}} = -78.43°$) for the second group. To verify that this solution is equivalent to the above solution, we plot the determinant of the information matrix as a function of ψ_3^{opt} given that $\psi_1^{\text{opt}} = 77.08°$, $\psi_4^{\text{opt}} = 102.92°$, $\psi_2^{\text{opt}} - \psi_3^{\text{opt}} = 81.91°$ and $\psi_5^{\text{opt}} - \psi_3^{\text{opt}} = -78.43°$ in Fig. 18. We observe that the determinant of the information matrix in Fig. 18 remains constant at the same value of $|\mathbf{M}_{\hat{\mathbf{p}}}| = 4.1821 \times 10^{-6}$ as that in Fig. 17, and therefore demonstrating that the optimality of the network geometry is not affected by different ways of grouping the sensors.

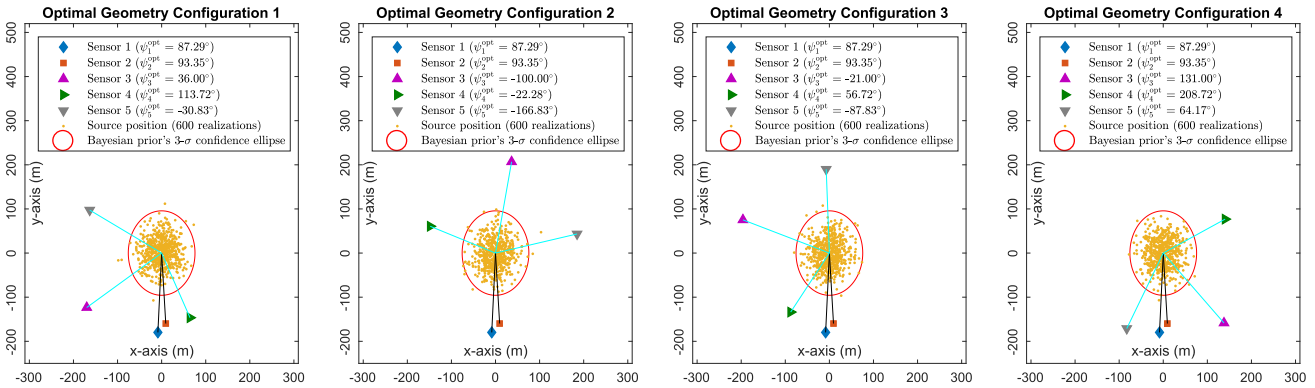

FIGURE 16. Examples of optimal geometry configurations for five RSS sensors with the parameter settings of $\mathbf{p}_0 = [0, 0]^T$ m, $\mathbf{C}_0 = \text{diag}\{636.2278, 1017.9644\}$ m^2, $\alpha_1 = \cdots = \alpha_5 = 3$, $d_1 = 180$ m, $d_2 = 160$ m, $d_3 = 210$ m, $d_4 = 160$ m, $d_5 = 190$ m, $\sigma_1 = 4$ dBm, $\sigma_2 = 5$ dBm, $\sigma_3 = 3$ dBm, $\sigma_4 = 4.5$ dBm and $\sigma_5 = 5$ dBm.

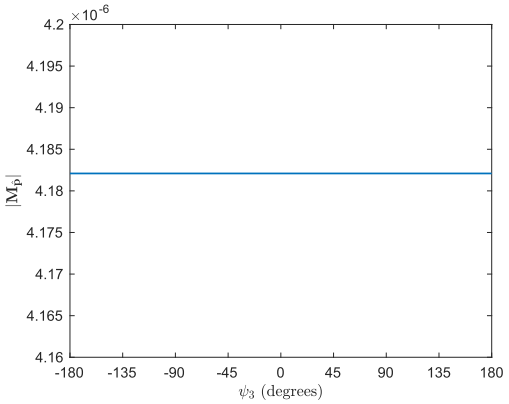

FIGURE 17. The determinant of information matrix $|\mathbf{M}_{\hat{\mathbf{p}}}|$ as a function of ψ_3 for five RSS sensors given that $\psi_1 = 87.29°$, $\psi_2 = 93.35°$, $\psi_4 - \psi_3 = 77.72°$ and $\psi_5 - \psi_3 = -66.83°$. Other parameter settings are given in Fig. 16.

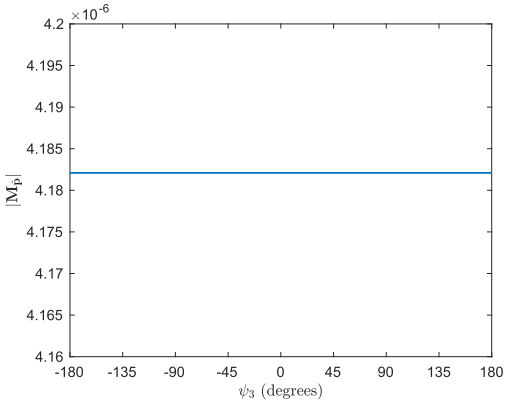

FIGURE 18. The determinant of information matrix $|\mathbf{M}_{\hat{\mathbf{p}}}|$ as a function of ψ_3 for five RSS sensors given that $\psi_1^{\text{opt}} = 77.08°$, $\psi_4^{\text{opt}} = 102.92°$, $\psi_2^{\text{opt}} - \psi_3^{\text{opt}} = 81.91°$ and $\psi_5^{\text{opt}} - \psi_3^{\text{opt}} = -78.43°$. Other parameter settings are given in Fig. 16.

D. MIXED SENSOR NETWORK

1) BEARING/RANGE NETWORK

In this simulation, we consider a mixed sensor network with two bearing sensors (sensors 1 and 2) and two range sensors (sensors 3 and 4). The simulation parameters include

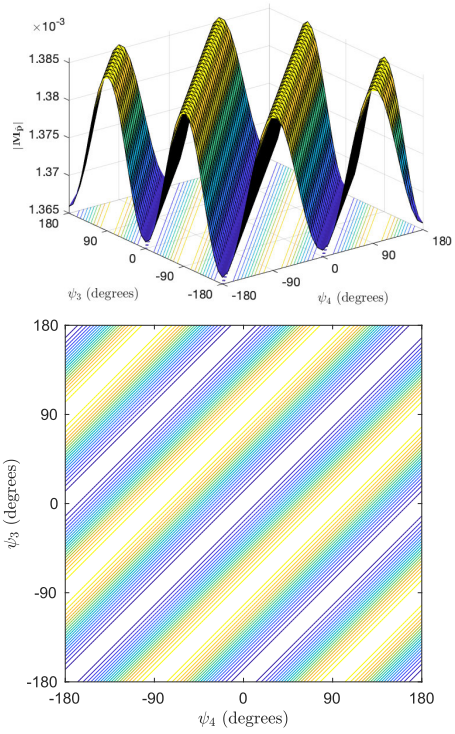

FIGURE 19. The determinant of information matrix $|\mathbf{M}_{\hat{\mathbf{p}}}|$ as a function of ψ_3 and ψ_4 for the case of a mixed sensor network with two bearing sensors (sensors 1 and 2) and two range sensors (sensors 3 and 4). Parameter settings: $\mathbf{p}_0 = [0, 0]^T$ m, $\mathbf{C}_0 = \text{diag}\{54.9065, 499.6487\}$ m^2, $d_1 = 270$ m, $d_2 = 240$ m, $d_3 = 200$ m, $d_4 = 250$ m, $\sigma_1 = \sigma_2 = 1.5°$, and $\sigma_3 = \sigma_4 = 15$ m. Here, we set $\psi_1^{\text{opt}} = -44.04°$ and $\psi_2^{\text{opt}} = -153.92°$.

$\mathbf{p}_0 = [0, 0]^T$ m, $\mathbf{C}_0 = \text{diag}\{54.9065, 499.6487\}$ m^2, $d_1 = 270$ m, $d_2 = 240$ m, $d_3 = 200$ m, $d_4 = 250$ m, $\sigma_1 = \sigma_2 = 1.5°$, and $\sigma_3 = \sigma_4 = 15$ m. To determine an optimal sensor placement, we cluster the sensors into two groups. Group 1 contains the two bearing sensors and the virtual sensor corresponding to the Bayesian prior, while Group 2 contains the two remaining range sensors. According to the analysis in Section III, an optimal angular arrangement for sensors 1 and 2 within Group 1 is given by $\psi_1^{\text{opt}} = -44.04°$

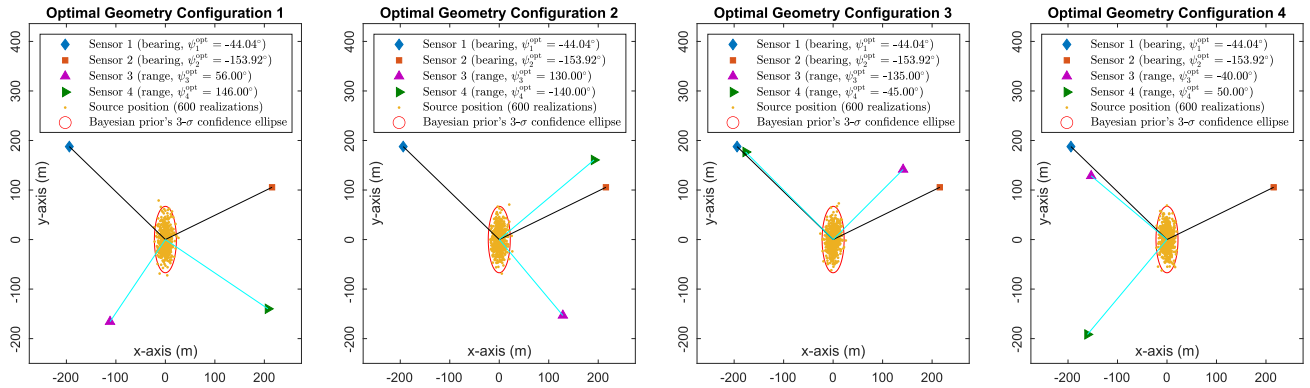

FIGURE 20. Examples of optimal geometry configurations for a mixed sensor network with two bearing sensors and two range sensors with the parameter settings given in Fig. 19.

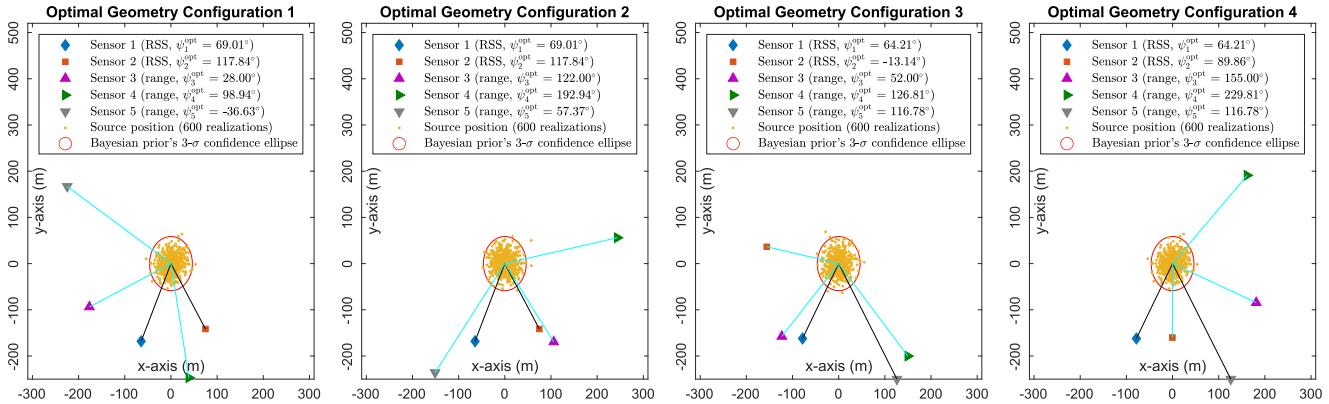

FIGURE 21. Example of optimal geometry configurations for a mixed sensor network with two RSS sensors and three range sensors (parameter settings are given in the text).

and $\psi_2^{\text{opt}} = -153.92°$, while the optimal arrangement for sensors 3 and 4 is governed by $|\psi_4^{\text{opt}} - \psi_3^{\text{opt}}| = 90°$. Using these results, by rotating Group 2, infinitely many optimal geometry configurations for the whole sensor network can be generated. To verify this, we set $\psi_1^{\text{opt}} = -44.04°$ and $\psi_2^{\text{opt}} = -153.92°$ and plot the determinant of the information matrix $|\mathbf{M}_{\hat{\mathbf{p}}}|$ as a function of ψ_3 and ψ_4 in Fig. 19. We observe that the values of ψ_3 and ψ_4 maximizing $|\mathbf{M}_{\hat{\mathbf{p}}}|$ forms a set of lines defined by $|\psi_4 - \psi_3| = 90°$. In other words, $|\mathbf{M}_{\hat{\mathbf{p}}}|$ is maximized when there is a 90° separation between ψ_3 and ψ_4 regardless of their actual values. This observation is congruent with the above analytical results.

Fig. 20 shows four examples of optimal sensor placement and the corresponding performance of the MAP estimator is reported in Table 10. We observe that the MAP estimator performs similarly across these geometries and its RMSE is quite close to the optimal RMSE value.

2) RSS/RANGE NETWORK

We now consider a mixed sensor network with two RSS sensors (sensors 1 and 2) and three range sensors (sensors 3, 4 and 5). We use the following parameters for this simulation: $\mathbf{p}_0 = [0, 0]^T$ m, $\mathbf{C}_0 = \text{diag}\{238.5854, 381.7367\}$ m^2, $\alpha_1 = \alpha_2 = 3$, $d_1 = 180$ m, $d_2 = 160$ m, $d_3 = 200$ m, $d_4 = 250$ m, $d_5 = 280$ m, $\sigma_1 = 2$ dBm, $\sigma_2 = 2.5$ dBm, $\sigma_3 = 22$ m, $\sigma_4 = 25$ m, and $\sigma_5 = 28$ m. Fig. 21 shows four examples of optimal sensor placement for the considered sensor network. Here, the first two geometry configurations are obtained by splitting the network into two groups: (i) group 1 with two RSS sensors and the virtual sensor corresponding to the Bayesian prior, and (ii) group 2 with the remaining three range sensors. Since the rotation between these two groups does not affect the optimality of the geometry for the whole network, we arbitrarily set $\psi_3^{\text{opt}} = 28°$ and 122° in configurations 1 and 2 respectively. On the other hand, configurations 3 and 4 are obtained by a different way

TABLE 10. Bias and RMSE Performance of the MAP Estimator for a Mixed Sensor Network With Two Bearing Sensors and Two Range Sensors Under the Optimal Geometries Shown in Fig. 20

Geometry	Bias norm	RMSE*
1	0.087 m	7.565 m
2	0.077 m	7.612 m
3	0.066 m	7.376 m
4	0.078 m	7.394 m

*Optimal RMSE = 7.330 m.

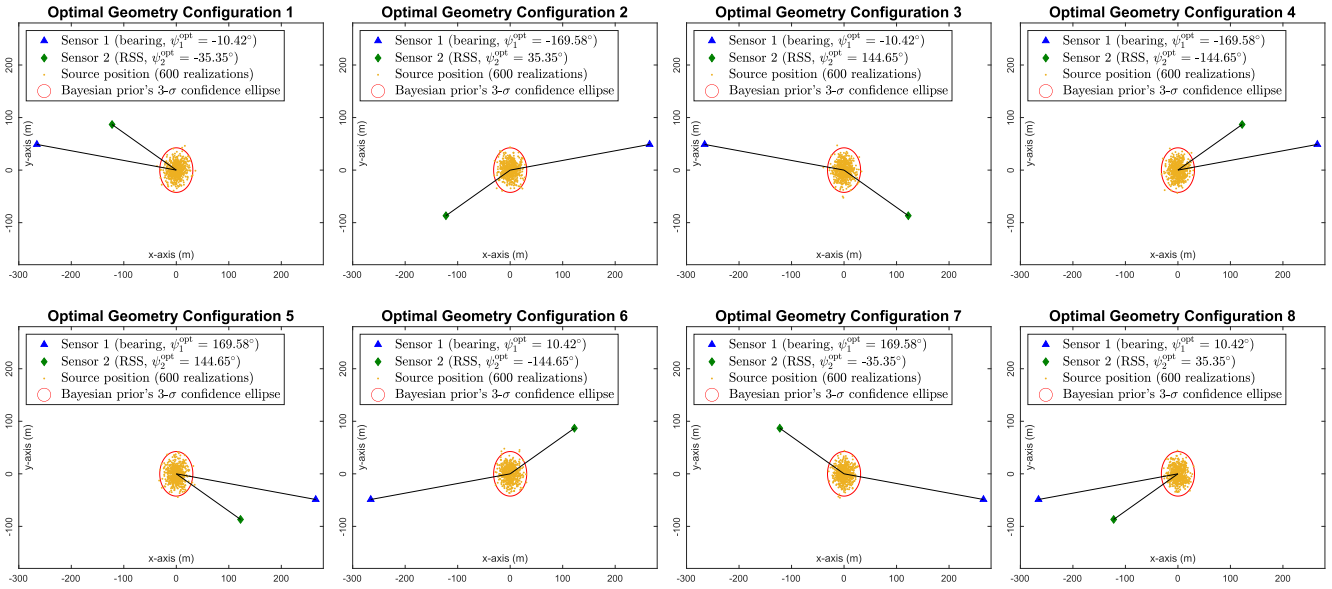

FIGURE 22. Optimal geometry configurations for a mixed sensor network with one bearing sensor and one RSS sensor (parameter settings are given in the text).

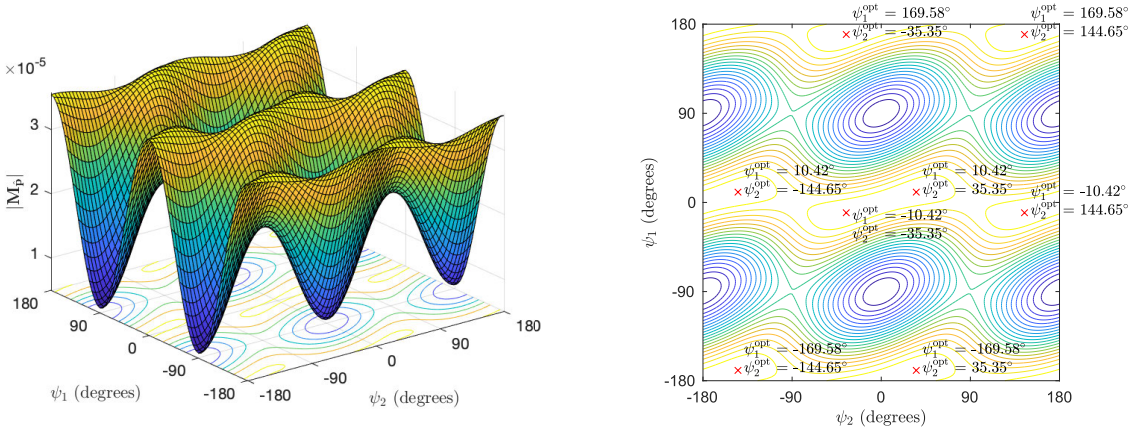

FIGURE 23. The determinant of information matrix $|\mathbf{M}_{\tilde{\mathbf{p}}}|$ as a function of ψ_1 and ψ_2 for a mixed sensor network with one bearing sensor and one RSS sensor. The maxima (indicated by '×') match the optimal geometry configurations in Fig. 22.

of splitting of the network: (i) group 1 with sensor 1 (RSS), sensor 5 (range) and the virtual sensor corresponding to the Bayesian prior, (ii) group 2 with sensor 2 (RSS), sensor 3 (range) and sensor 4 (range). Here, we arbitrarily set $\psi_3^{\text{opt}} = 52°$ in configuration 3 and $\psi_3^{\text{opt}} = 155°$ in configuration 4 without affecting the optimality of the network geometry. Note that these four geometry configurations are equivalently optimal and share the same optimal RMSE value of 16.829 m. Table 11 reports the bias and RMSE performance of the MAP estimator under these geometry conditions, where a similar performance of the MAP estimator is observed and its RMSE agrees well with the optimal RMSE value.

3) BEARING/RSS NETWORK

This example considers a mixed sensor network with one bearing sensor (sensor 1) and one RSS sensor (sensor 2)

TABLE 11. Bias and RMSE Performance of the MAP Estimator for a Mixed Sensor Network With Two RSS Sensors and Three Range Sensors Under the Optimal Geometries Shown in Fig. 21

Geometry	Bias norm	RMSE⋆
1	0.215 m	16.806 m
2	0.169 m	16.843 m
3	0.201 m	16.842 m
4	0.322 m	16.850 m

⋆Optimal RMSE = 16.829 m.

with the following parameter settings: $\mathbf{p}_0 = [0, 0]^T$ m, $\mathbf{C}_0 = \text{diag}\{110.4196, 199.8595\}$ m^2, $\sigma_1 = 3°$, $d_1 = 270$ m, $\alpha_2 = 3$, $\sigma_2 = 2$ dBm, and $d_2 = 150$ m. In this example, the condition (31) is satisfied. Thus, the solution for the optimal angular placement of the sensors can be obtained from (26) and (36). This leads to 8 configurations shown in

TABLE 12. Bias and RMSE Performance of the MAP Estimator for a Mixed Sensor Network With One Bearing Sensor and One RSS Sensor Under the Optimal Geometries Shown in Fig. 22

Geometry	Bias norm	RMSE*
1	0.278 m	13.836 m
2	0.080 m	13.821 m
3	0.079 m	13.845 m
4	0.277 m	13.846 m
5	0.278 m	13.821 m
6	0.081 m	13.797 m
7	0.080 m	13.831 m
8	0.274 m	13.820 m

*Optimal RMSE = 13.818 m.

Fig. 22, which match the maxima on the plot of $|\mathbf{M}_{\hat{\mathbf{p}}}|$ as shown in Fig. 23; thus confirming the accuracy of the analytical geometry solution. Under these optimal geometries, the MAP estimator is observed in Table 12 to produce a RMSE performance closely agreeing with the optimal analytical RMSE of 13.818 m.

V. CONCLUSION

We have presented an optimal geometry analysis for the problem of target localization with Bayesian priors. Our analysis was conducted in a unified manner and can be applied to different types of sensor networks including bearing-only network, range-only network, RSS-only network and mixed network of these sensor types. The A-optimality and D-optimality criteria for geometry optimization of Bayesian target localization was shown to be equivalent (see Theorem 1). Under these optimality criteria, it was established in Theorem 2 that the geometry optimization problem essentially becomes the vector sum modulus minimization problem. This is an important result as it makes the computation of the optimal geometry conditions algebraically simple. Finally, the analytical findings of the article were verified via a range of numerical simulation studies, where a good agreement between the analytical and numerical results was observed.

APPENDIX A

By substituting (10) into (12), the information matrix becomes

$$\mathbf{M}_{\hat{\mathbf{p}}} = \mathbf{M}_0 + \sum_{k=1}^{N} \frac{1}{\sigma_k^2} \mathbf{J}_k^T \mathbf{J}_k. \tag{39}$$

In what follows, we will derive the expression of $\frac{1}{\sigma_k^2}\mathbf{J}_k^T\mathbf{J}_k$ for bearing, range and RSS sensors respectively.

If sensor k is a bearing sensor, $\mathbf{J}_k$ in (11) is given by

$$\mathbf{J}_k = \frac{1}{d_k}\left[-\sin\psi_k, \cos\psi_k\right], \tag{40}$$

and thus we obtain

$$\frac{1}{\sigma_k^2}\mathbf{J}_k^T\mathbf{J}_k = \frac{1}{\sigma_k^2 d_k^2}\begin{bmatrix}-\sin\psi_k \\ \cos\psi_k\end{bmatrix}\left[-\sin\psi_k, \cos\psi_k\right]. \tag{41}$$

By defining

$$c_k^2 = \frac{1}{\sigma_k^2 d_k^2},\ \theta_k = \psi_k + \frac{\pi}{2}, \tag{42}$$

and

$$\mathbf{u}_k = [\cos\theta_k, \sin\theta_k]^T, \tag{43}$$

the expression in (41) becomes

$$\frac{1}{\sigma_k^2}\mathbf{J}_k^T\mathbf{J}_k = c_k^2\begin{bmatrix}\cos\theta_k \\ \sin\theta_k\end{bmatrix}\left[\cos\theta_k, \sin\theta_k\right] = c_k^2\mathbf{u}_k\mathbf{u}_k^T. \tag{44}$$

If sensor k is a range sensor, $\mathbf{J}_k$ in (11) is given by

$$\mathbf{J}_k = \left[\cos\psi_k, \sin\psi_k\right], \tag{45}$$

and thus we obtain

$$\frac{1}{\sigma_k^2}\mathbf{J}_k^T\mathbf{J}_k = \frac{1}{\sigma_k^2}\begin{bmatrix}\cos\psi_k \\ \sin\psi_k\end{bmatrix}\left[\cos\psi_k, \sin\psi_k\right]. \tag{46}$$

By defining

$$c_k^2 = \frac{1}{\sigma_k^2},\quad \theta_k = \psi_k, \tag{47}$$

the expression in (46) can be rewritten as

$$\frac{1}{\sigma_k^2}\mathbf{J}_k^T\mathbf{J}_k = c_k^2\mathbf{u}_k\mathbf{u}_k^T. \tag{48}$$

If sensor k is a RSS sensor, $\mathbf{J}_k$ in (11) is given by

$$\mathbf{J}_k = -\frac{10\alpha_k}{\ln(10)d_k}\left[\cos\psi_k, \sin\psi_k\right], \tag{49}$$

and thus we obtain

$$\frac{1}{\sigma_k^2}\mathbf{J}_k^T\mathbf{J}_k = \frac{100\alpha_k^2}{\ln^2(10)\sigma_k^2 d_k^2}\begin{bmatrix}\cos\psi_k \\ \sin\psi_k\end{bmatrix}\left[\cos\psi_k, \sin\psi_k\right]. \tag{50}$$

By defining

$$c_k^2 = \frac{100\alpha_k^2}{\ln^2(10)\sigma_k^2 d_k^2},\quad \theta_k = \psi_k, \tag{51}$$

the expression in (50) becomes

$$\frac{1}{\sigma_k^2}\mathbf{J}_k^T\mathbf{J}_k = c_k^2\mathbf{u}_k\mathbf{u}_k^T. \tag{52}$$

Using the results in (40)–(52), the information matrix in (39) can be written in a compact form as

$$\mathbf{M}_{\hat{\mathbf{p}}} = \mathbf{M}_0 + \sum_{k=1}^{N} c_k^2\mathbf{u}_k\mathbf{u}_k^T \tag{53}$$

where

$$c_k^2 = \begin{cases} \dfrac{1}{\sigma_k^2 d_k^2} & \text{if sensor } k \text{ is a bearing sensor} \\ \dfrac{1}{\sigma_k^2} & \text{if sensor } k \text{ is a range sensor} \\ \dfrac{100\alpha_k^2}{\ln^2(10)\sigma_k^2 d_k^2} & \text{if sensor } k \text{ is a RSS sensor,} \end{cases} \tag{54}$$

$$|\mathbf{M}_{\hat{\mathbf{p}}}| = \mathbf{M}_{\hat{\mathbf{p}}}(1,1)\mathbf{M}_{\hat{\mathbf{p}}}(2,2) - \mathbf{M}_{\hat{\mathbf{p}}}(1,2)\mathbf{M}_{\hat{\mathbf{p}}}(2,1) \tag{57a}$$

$$= \left(A + \frac{1}{2}\sum_{k=1}^{N} c_k^2(1+\cos 2\theta_k)\right)\left(B + \frac{1}{2}\sum_{k=1}^{N} c_k^2(1-\cos 2\theta_k)\right) - \left(\frac{1}{2}\sum_{k=1}^{N} c_k^2 \sin 2\theta_k\right)^2 \tag{57b}$$

$$= AB + \frac{A}{2}\sum_{k=1}^{N} c_k^2 - \frac{A}{2}\sum_{k=1}^{N} c_k^2\cos 2\theta_k + \frac{B}{2}\sum_{k=1}^{N} c_k^2 + \frac{B}{2}\sum_{k=1}^{N} c_k^2\cos 2\theta_k$$
$$+\frac{1}{4}\sum_{k=1}^{N} c_k^2(1+\cos 2\theta_k)\sum_{k=1}^{N} c_k^2(1-\cos 2\theta_k) - \frac{1}{4}\left(\sum_{k=1}^{N} c_k^2 \sin 2\theta_k\right)^2 \tag{57c}$$

$$= AB + \frac{(A+B)}{2}\sum_{k=1}^{N} c_k^2 + \frac{(B-A)}{2}\sum_{k=1}^{N} c_k^2\cos 2\theta_k$$
$$+\frac{1}{4}\left(\sum_{k=1}^{N} c_k^2\right)^2 - \frac{1}{4}\left(\sum_{k=1}^{N} c_k^2\cos 2\theta_k\right)^2 - \frac{1}{4}\left(\sum_{k=1}^{N} c_k^2 \sin 2\theta_k\right)^2 \tag{57d}$$

$$= AB + \frac{(A+B)}{2}\sum_{k=1}^{N} c_k^2 + \frac{1}{4}\left(\sum_{k=1}^{N} c_k^2\right)^2 + \left(\frac{A-B}{2}\right)^2$$
$$-\frac{1}{4}\left(\sum_{k=1}^{N} c_k^2\cos 2\theta_k\right)^2 - \frac{(A-B)}{2}\sum_{k=1}^{N} c_k^2\cos 2\theta_k - \left(\frac{A-B}{2}\right)^2$$
$$-\frac{1}{4}\left(\sum_{k=1}^{N} c_k^2 \sin 2\theta_k\right)^2 \tag{57e}$$

$$= AB + \frac{(A+B)}{2}\sum_{k=1}^{N} c_k^2 + \frac{1}{4}\left(\sum_{k=1}^{N} c_k^2\right)^2 + \left(\frac{A-B}{2}\right)^2$$
$$-\frac{1}{4}\left((A-B) + \sum_{k=1}^{N} c_k^2\cos 2\theta_k\right)^2 - \frac{1}{4}\left(\sum_{k=1}^{N} c_k^2 \sin 2\theta_k\right)^2. \tag{57f}$$

and $\mathbf{u}_k = [\cos\theta_k, \sin\theta_k]^T$ with

$$\theta_k = \begin{cases} \psi_k + \dfrac{\pi}{2} & \text{if sensor } k \text{ is a bearing sensor} \\ \psi_k & \text{if sensor } k \text{ is a range sensor} \\ \psi_k & \text{if sensor } k \text{ is a RSS sensor.} \end{cases} \tag{55}$$

APPENDIX B

By substituting (21) into (19), the entries of the information matrix becomes

$$\mathbf{M}_{\hat{\mathbf{p}}}(1,1) = A + \sum_{k=1}^{N} c_k^2\cos^2\theta_k$$
$$= A + \frac{1}{2}\sum_{k=1}^{N} c_k^2(1+\cos 2\theta_k), \tag{56a}$$

$$\mathbf{M}_{\hat{\mathbf{p}}}(1,2) = \mathbf{M}_{\hat{\mathbf{p}}}(2,1)$$
$$= \sum_{k=1}^{N} c_k^2 \sin\theta_k\cos\theta_k$$
$$= \frac{1}{2}\sum_{k=1}^{N} c_k^2 \sin 2\theta_k, \tag{56b}$$

$$\mathbf{M}_{\hat{\mathbf{p}}}(2,2) = B + \sum_{k=1}^{N} c_k^2\sin^2\theta_k$$
$$= B + \frac{1}{2}\sum_{k=1}^{N} c_k^2(1-\cos 2\theta_k). \tag{56c}$$

Using these results, the determinant of $\mathbf{M}_{\hat{\mathbf{p}}}$ is derived as in (57), as shown at the top of the page, where the final expression of $|\mathbf{M}_{\hat{\mathbf{p}}}|$ in (57f) is identical to that given in (23).

REFERENCES

[1] A. N. Bishop, B. Fidan, B. D. O. Anderson, K. Doğançay, and P. N. Pathirana, "Optimality analysis of sensor-target localization geometries," *Automatica*, vol. 46, no. 3, pp. 479–492, Mar. 2010.
[2] S. Zhao, B. M. Chen, and T. H. Lee, "Optimal sensor placement for target localisation and tracking in 2D and 3D," *Int. J. Control*, vol. 86, no. 10, pp. 1687–1704, Oct. 2013.
[3] N. H. Nguyen and K. Dogancay, *Signal Processing for Multistatic Radar Systems: Adaptive Waveform Selection, Optimal Geometries and Pseudo-linear Tracking Algorithms*. London, U.K.: Academic, 2019.

[4] S. Zhao, B. M. Chen, and T. H. Lee, "Optimal deployment of mobile sensors for target tracking in 2D and 3D spaces," *IEEE/CAA J. Autom. Sinica*, vol. 1, no. 1, pp. 24–30, Jan. 2014.
[5] Y. Oshman and P. Davidson, "Optimization of observer trajectories for bearings-only target localization," *IEEE Trans. Aerosp. Electron. Syst.*, vol. 35, no. 3, pp. 892–902, Jul. 1999.
[6] J. Ousingsawat and M. E. Campbell, "Optimal cooperative reconnaissance using multiple vehicles," *J. Guid., Control, Dyn.*, vol. 30, no. 1, pp. 122–132, 2007.
[7] N. H. Nguyen, K. Dogancay, and L. M. Davis, "Joint transmitter waveform and receiver path optimization for target tracking by multistatic radar system," in *Proc. IEEE Workshop Stat. Signal Process. (SSP)*, Gold Coast, QLD, Australia, Jun. 2014, pp. 444–447.
[8] S. Martínez and F. Bullo, "Optimal sensor placement and motion coordination for target tracking," *Automatica*, vol. 42, no. 4, pp. 661–668, Apr. 2006.
[9] K. Doğançay and H. Hmam, "Optimal angular sensor separation for AOA localization," *Signal Process.*, vol. 88, no. 5, pp. 1248–1260, May 2008.
[10] S. Zhao, B. M. Chen, and T. H. Lee, "Optimal placement of bearing-only sensors for target localization," in *Proc. Amer. Control Conf. (ACC)*, Montreal, QC, Canada, Jun. 2012, pp. 5108–5113.
[11] A. N. Bishop, B. Fidan, B. D. O. Anderson, K. Dogancay, and P. N. Pathirana, "Optimality analysis of sensor-target geometries in passive localization: Part 1–Bearing-Only localization," in *Proc. 3rd Int. Conf. Intell. Sensors, Sensor Netw. Inf.*, Melbourne, VIC, Australia, 2007, pp. 7–12.
[12] Y. Liang and Y. Jia, "Constrained optimal placements of heterogeneous Range/Bearing/RSS sensor networks for source localization with distance-dependent noise," *IEEE Geosci. Remote Sens. Lett.*, vol. 13, no. 11, pp. 1611–1615, Nov. 2016.
[13] N. H. Nguyen and K. Dogancay, "Optimal geometry analysis for multistatic TOA localization," *IEEE Trans. Signal Process.*, vol. 64, no. 16, pp. 4180–4193, Aug. 2016.
[14] N. H. Nguyen and K. Dogancay, "Optimal geometry analysis for elliptic target localization by multistatic radar with independent bistatic channels," in *Proc. IEEE Int. Conf. Acoust., Speech Signal Process. (ICASSP)*, Brisbane, QLD, Australia, Apr. 2015, pp. 2764–2768.
[15] M. Sadeghi, F. Behnia, and R. Amiri, "Optimal sensor placement for 2-D range-only target localization in constrained sensor geometry," *IEEE Trans. Signal Process.*, vol. 68, pp. 2316–2327, 2020.
[16] A. N. Bishop, B. Fidan, B. D. O. Anderson, P. N. Pathirana, and K. Dogancay, "Optimality analysis of sensor-target geometries in passive localization: Part 2–Time-of-Arrival based localization," in *Proc. 3rd Int. Conf. Intell. Sensors, Sensor Netw. Inf.*, Melbourne, VIC, Australia, 2007, pp. 13–18.
[17] L. Rui and K. C. Ho, "Elliptic localization: Performance study and optimum receiver placement," *IEEE Trans. Signal Process.*, vol. 62, no. 18, pp. 4673–4688, Sep. 2014.
[18] S. Xu, Y. Ou, and X. Wu, "Optimal sensor placement for 3-D time-of-arrival target localization," *IEEE Trans. Signal Process.*, vol. 67, no. 19, pp. 5018–5031, Oct. 2019.
[19] K. Dogancay and H. Hmam, "On optimal sensor placement for time-difference-of-arrival localization utilizing uncertainty minimization," in *Proc. Eur. Signal Process. Conf. (EUSIPCO)*, Glasgow, U.K., 2009, pp. 1136–1140.
[20] K. W. K. Lui and H. C. So, "A study of two-dimensional sensor placement using time-difference-of-arrival measurements," *Digit. Signal Process.*, vol. 19, no. 4, pp. 650–659, Jul. 2009.
[21] A. N. Bishop and P. Jensfelt, "An optimality analysis of sensor-target geometries for signal strength based localization," in *Proc. Int. Conf. Intell. Sensors, Sensor Netw. Inf. Process. (ISSNIP)*, Melbourne, Australia, Dec. 2009, pp. 127–132.
[22] N. H. Nguyen and K. Dogancay, "Optimal sensor placement for Doppler shift target localization," in *Proc. IEEE Radar Conf. (RadarCon)*, Arlington, VA, USA, May 2015, pp. 1677–1682.
[23] N. H. Nguyen and K. Dogangay, "Optimal sensor-target geometries for Doppler-shift target localization," in *Proc. 23rd Eur. Signal Process. Conf. (EUSIPCO)*, Nice, France, Aug. 2015, pp. 180–184.
[24] W. Meng, L. Xie, and W. Xiao, "Optimality analysis of sensor-source geometries in heterogeneous sensor networks," *IEEE Trans. Wireless Commun.*, vol. 12, no. 4, pp. 1958–1967, Apr. 2013.
[25] C. Yang, L. Kaplan, E. Blasch, and M. Bakich, "Optimal placement of heterogeneous sensors for targets with Gaussian priors," *IEEE Trans. Aerosp. Electron. Syst.*, vol. 49, no. 3, pp. 1637–1653, Jul. 2013.
[26] C. Yang, L. Kaplan, E. Blasch, and M. Bakich, "Optimal placement of heterogeneous sensors in target tracking," in *Proc. Int. Conf. Inform. Fusion*, Chicago, IL, USA, 2011, pp. 1–8.
[27] C. Yang, L. Kaplan, and E. Blasch, "Performance measures of covariance and information matrices in resource management for target state estimation," *IEEE Trans. Aerosp. Electron. Syst.*, vol. 48, no. 3, pp. 2594–2613, Jul. 2012.
[28] S. M. Kay, *Fundamentals of Statistical Signal Processing: Estimation Theory*. Englewood Cliffs, NJ, USA: Prentice-Hall, 1993.
[29] H. L. Van Trees, K. L. Bell, and Z. Tian, *Detection, Estimation, and Modulation Theory: Detection, Estimation, and Filtering Theory*, 2nd ed. Hoboken, NJ, USA: Wiley, 2013.
[30] L. Ljung and T. Soderstrom, *Theory and Practice of Recursive Identification*. Cambridge, MA, USA: MIT Press, 1983.
[31] S. Haykin, *Adaptive Filter Theory*, 3rd ed. Englewood Cliffs, NJ, USA: Prentice-Hall, 1996.
[32] J. A. Nelder and R. Mead, "A simplex method for function minimization," *Comput. J.*, vol. 7, no. 4, pp. 308–313, Jan. 1965.
[33] N. H. Nguyen and K. Dogancay, "Closed-form algebraic solutions for Angle-of-Arrival source localization with Bayesian priors," *IEEE Trans. Wireless Commun.*, vol. 18, no. 8, pp. 3827–3842, Aug. 2019.

NGOC HUNG NGUYEN (Member, IEEE) received the B.E. degree (Hons.) in electrical and electronic engineering from The University of Adelaide, Australia, in 2012, and the Ph.D. degree in telecommunications from the University of South Australia, Australia, in 2016. From 2016 to 2018, he was a Research Fellow and a Lecturer with the University of South Australia. He is currently a Researcher with the Defence Science and Technology (DST) Group, Australia, and also an Adjunct Research Fellow with the University of South Australia. He is the first author of a book *Signal Processing for Multistatic Radar Systems: Adaptive Waveform Selection, Optimal Geometries and Pseudolinear Tracking Algorithms* (London, U.K.: Academic Press, 2019). His research interests include statistical and adaptive signal processing, compressive sensing, and estimation theory with emphasis on target localization and tracking, sensor management, and radar imaging.

Dr. Nguyen currently serves as the Chair for the IEEE South Australia Communications and Signal Processing Chapter. He also serves on the Editorial Board of *Digital Signal Processing*.